MONITORING AND MODELLING OF PHYTOPLANKTON DISTRIBUTION IN AN ARTIFICIAL WETLAND USING HIGH-RESOLUTION SATELLITE IMAGERY: A CASE STUDY OF KRISTALBAD, ENCHEDE, NL

YUMENG SONG
February, 2016

SUPERVISORS:
Dr.ir. C.M.M. Mannaerts
Dr.ir. S. Salama

MONITORING AND MODELLING OF PHYTOPLANKTON DISTRIBUTION IN AN ARTIFICIAL WETLAND USING HIGH-RESOLUTION SATELLITE IMAGERY: A CASE STUDY OF KRISTALBAD, ENCHEDE, NL

[YUMENG SONG]
Enschede, The Netherlands, [February, 2016]

Thesis submitted to the Faculty of Geo-Information Science and Earth Observation of the University of Twente in partial fulfilment of the requirements for the degree of Master of Science in Geo-information Science and Earth Observation.
Specialization: Water Resources and Environment Management

SUPERVISORS:
Dr.ir. C.M.M. Mannaerts
Dr.ir. S. Salama

THESIS ASSESSMENT BOARD:
Prof. Dr. ing. W. Verhoe
Prof. Dr. X. Wang (External Examiner, Capital Normal University)
Dr.ir. C.M.M. Mannaerts
Dr.ir. S. Salama

ABSTRACT

Kristalbad is an artificial wetland, and contains various aquatic phytoplankton communities play a role in further purifying effluent waters from the WWTP Enschede-West, flowing in the Elsbeek. It is therefore very important to monitor the dynamic changes of the plankton and their roles in removing nutrients and other chemicals. However, high resolution image platforms are needed which are able to view the wetland with both high spatial and high temporal resolutions. SPOT6 is high resolution (＜10 m) satellite dedicated to site surveillance with a high spatial resolution sensor set on a frequent revisit orbit (1.5 m in panchromatic and 6 m in multispectral). In the first part of this research, we integrated the filed hyperspectral data collected from the TriOS Ramses and the field measured Chl-*a* data, and then develop a best-fitted band ratio empirical algorism (blue-red-NIR) to generate the distribution map of concentrations of Chlorophyll-a (Chl-a) from the Spot 6 image. Then we compared the Chl-a concentration retrieved from remote sensing with an eutrophication model (EUTRO1) which we setup for the wetland pond system for a given period. Our study allowed join correlation between RS, water quality modelling and in-situ data. More field data and time series satellite data are helped to fully confirm here promoting our findings.

KEYWORDS
SPOT 6, phytoplankton, eco-hydraulic modelling, artificial wetlands, eutrophication

ACKNOWLEDGEMENTS

I would like to have this opportunity to express my sincere gratitude to people who offer support for my MSc study and research during the 15 months staying ITC, University of Twente; 15 months staying in Capital Normal university. Without these help, this research would not be possible.

First I would like to express my profound gratitude to Dr. Chris Mannaerts my first supervisor and a special person with a great heart, for his tremendous support and intelligent guidance during whole my research period. At the same time, I want to say thank you to my second supervisor, Dr. Suhyb .Salama, who gave me a lot of useful advice and encouragement.

I also want to express my grateful to Dr. Caroline Lievens, she is a very kind and patient for helping me with the laboratory analysis.

I am deeply grateful for all the stuffs of WREM program, for the rigorous scientific attitude and enthusiastic lectures. I learned a lot form their advanced demonstration and classes, these would be my unforgettable valuable intellectual treasure in my life.

I appreciate all my friends and classmates in ITC, for good company and encouragement. Special thanks to my classmates, Justin, Mujeeb, Christian, Peter for helping me to do the field work. I also want to say thank you to our 7 person team from Capital Normal University. Meanwhile, I want to express my deeply grateful to my friends for supporting and encouraging me during my MSc period, including Yancheng Wang, Jiawei Zhang and Wei Wang.

Special thanks to my boyfriend Yizhen for technical supporting, love, and encouragement. I will never forget the time and happiness to be with you.

Finally, I want to give my thanks to my father and mother for their honourable support, encouragements and love.

TABLE OF CONTENTS

LIST OF FIGURES

LIST OF TABLES

LIST OF APPENDIX

ABBREVIATION

Chl-*a*	Chlorophyll-a
C_{chla}	Concentration of Chlorophyll-a
CDOM	Colored Dissolved Organic Matter
DN	Digital Number
DEM	Digital Elevation Model
DMS	Duflow Modeling Studio
ETM	Enhanced Thematic Mapper
FORMOSAT	福尔摩沙
FLAASH	Fast Line- of-sight Atmospheric Analysis of Spectral Hypercubes
GIS	Geographic Information System
GPS	Global Positional System
ITC	International Institute of Geo-Information Science and Earth Observation
IOPs	Inherent Optical Properties
NIR	Near Infrared band
VIS	Visible band
MS	Multispectral band
PAN	Panchromatic band
KNMI	Royal Netherlands Meteorological Institute
MODTRAN	Moderate Resolution Atmospheric Transmission
SK	Site od Kristalbad
SNR	Signal-to-Noise Ratio
SPM	Suspended matter
SDV	Standard deviation
R_{rs}	Remote Sensing Reflectance
RPC	Rational Polynomial Coefficient
RMSE	Root Mean Square Error
RPD	Relative Percentage Deviation
SPOT	Satellite for Observation of Earth
STP	Sewage Treatment Plant
RSI	Remote Sensing Imager
WWTP	Waste Water Treatment Plant

1. INTRODUCTION

1.1. Background

Constructed wetlands are the one of the efficient methods for treating polluted water containing high nutrients and this capacity is well described.(Emy Chan, Taras A. Bursztynsky, Norman Hantzsche, 1982; Res et al., 1983; Vymazal, 2007) Wetlands and wetlands are mainly built to purify water to an acceptable quality.

In the Netherlands, wetlands are applied more and more often on a basis of the water harmonica concept. Between the water cycle and the water system is a water gap (see figure 1-1). To bridge this gap placed a wetland between the water cycle and the water system, the water harmonica (van den Trees & Kampf, 2013). A water harmonica is usually fully or partially fed with effluent that comes from a sewage treatment plant (STP). A water harmonica often consists of many ponds with reed ditches as the habitat for fish. Then transfer the " catalogued " water in the surface water system (van Herpen, Schomaker, Boosts, Kampf and Claassen, 2014).

In the past 20 years there are fifteen water harmonicas built in the Netherlands (van den Trees & Kampf, 2013). One of these water harmonicas is Kristalbad between Enschede and Hengelo (Overijssel). The “Kristalbad” is a recently constructed artificial wetland which came into use in 2012-2013, located between Hengelo and Enschede (Figure1-2). It is a complex but challenging water management project because multiple water functions and ecosystem services are combined in such a limited area which are respectively storm water retention, water quality improvement, ecological connect, recreational (walking and bird watching, etc.) and landscape management. The input water in the Kristalbad comes largely from the urban sewage treatment plant effluent of Enschede-West which contains the nutrients, organic matter and other pollutants, flows into the Elsbeek.

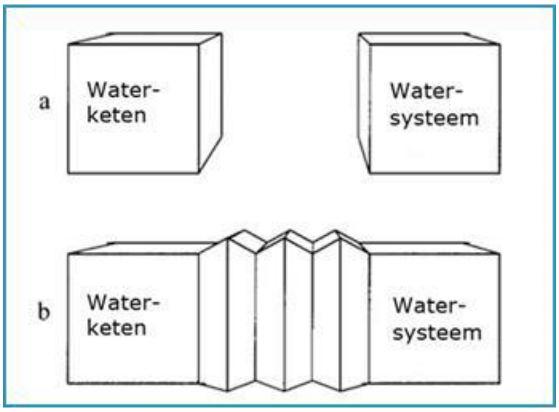

Figure 1-1 Principle of a water harmonica; a. the quality gap between the water cycle and watersystem, b. a water harmonica is disposed between the water-water system and the water quality in order to bridge the gap.(van den Boomen & Kampf, 2013)

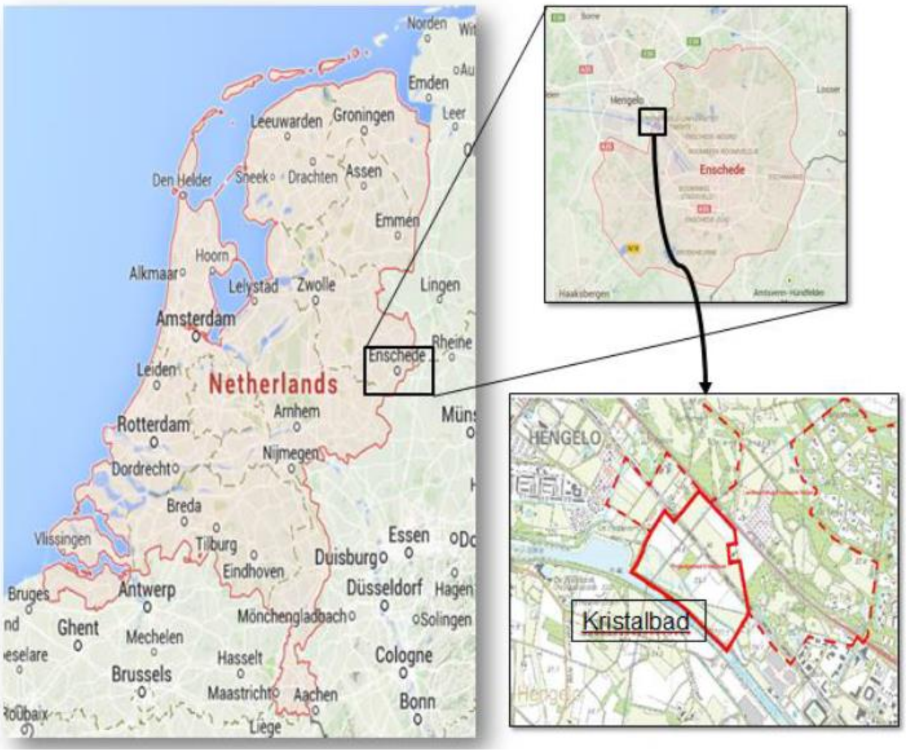

Figure 1-2 Geographical location of the Kristalbad

This "water machine" was built for storm water retention and also intended to improve the water quality of the Elsbeek and downstream Bornsebeek systems. (It was inspired by proven methods of the Wetland Research Centre at the University of Halmstad in Sweden). Also, the pond compartments of Kristalbad are filled up alternately undergoing a diurnal filling – and - drainage cycle and under the influence of light and air, biogeochemical processes in the water and sediment and aquatic vegetation, there will be a purifying effect like breaking down and converting nutrients, carbon and other substances. But as these years, the increasing human activities, domestic wastewater and industrial policies lead to drastically increases in the urban sewage emissions, also the nutrients loading of the Kristalbad. This may affect the ecological health and functional of Kristalbad. Therefore, it is necessary to monitoring the dynamic changes of the Kristalbad.

1.2. Research Objectives

The main objective of this research is to characterize the spatial distribution of phytoplankton chlorophyll-a , then to simulate and predict their dynamic change in Kristalbad.

The specific objectives are the following:

- Determine the relationship between the chlorophyll-a concentration and spectra properties using field spectrometry and water sampling.
- To map the spatial distribution of phytoplankton through integrating the field spectrometry, SPOT6 image and water sampling
- To build a prototype eco-hydraulic model to simulate hydrologic behavior of the Kristalbad constructed wetlands.
- To build a water quality prediction model to simulate and predict the chlorophyll-a concentration changes under certain period of the Kristalbad constructed wetlands.

1.3. Research Problem

Phytoplankton is an important component of the vegetation species of the wetland for purifying the waste water. There is a mutually beneficial relation between the bacteria and dominant phytoplankton community in the ponds of wetland. And the dominant phytoplankton community plays an important and complex role in removing the nutrients, organic matter and other pollutants.(Gersberg, Elkins, Lyon, & Goldman, 1986; Iamchaturapatr, Yi, & Rhee, 2007) Phytoplankton likes the trees and grass, utilize the solar energy through the photosynthesis to produce the biomass and release the oxygen.(Falkowski, 1994) Phytoplankton photosynthesis forms nearly all food sources for the aquatic live and could be considered as the mainly impact on the productivity of aquatic environment. Phytoplankton also are excellent indicators of ecological change, they are very sensitive to the nutrients, especially the concentration of nitrogen and phosphorus. When the nutrients overloading occurs in an ecosystem, it will led the phytoplankton excessive growth. Often in eutrophic ecosystem, it will be dominated by cyanobacteria, and may produce toxins, harm to public health.(Anderson, Glibert, & Burkholder, 2002a) For these reasons, studies of the population dynamics of phytoplankton are of great interest.

Chlorophyll is the main pigment in the phytoplankton cells, however, reckoning of chlorophyll-a (Chl-*a*) concentration (C_{chla}) in optically shallow water is not much straightforward due to its high seasonal variation.(Hole & Brook, 1982) In order to continuous and intensive water quality management in the wetland reserve such as the Kristalbad, integrating in situ sampling, modelling, and also remote sensing could help to lower the costs and time spends of measurement, and provide complementary results.(Dekker, Hoogenboom, Goddijn, & Malthus, 1997) Moreover, with the help of the water quality modelling, we can forecast the Chl-*a* concentration dynamics under certain hydraulic conditions and in the certain period.(Hamilton & Schladow, 1997)

However, several questions in relation to its functioning, sustainability and impact still need to be answered. The hydraulic management (cycles) affect the purification capacity of the system, growth of aquatic vegetation and the retention of other substances such as heavy metals, dissolved and particulate carbon still need us to detect and observe. The medium long term condition of the suspended matter coming from the Elsbeek and settling in the ponds, decomposition of aquatic weeds also need us to find a good way to monitor these changes. Also it is necessary to estimate the sensitivity and resilience of the system to externalities such as extreme weather events, high or low chemical loadings. Geospatial and high resolution satellite data such as FORMOSAT-2, SOPT-6 and LANDSAT-8 may help with remote monitoring these water systems in additional to the traditional analysis approach under the simplified hydrologic model DUFLOW.

The present MSc studies will address a number of specific questions as phrased above. The research will be done in close cooperation with the regional water authority "WaterschapVechstromen" and the municipality (Enschede city) in relation to the WWTP management.

In this study, focus was given to monitor the distribution of phytoplankton concentration which have been regarded as a deliberated approach for (contains high nutrients) purification is utilizing the wetlands (both natural and artificial). Wetlands as biological treatment systems, which contain various phytoplankton are used for treating the water and purifying polluted water from high nutrients. (Iamchaturapatr, Yi, & Rhee, 2007) At the same time, this method contains biological, physical and chemical complex processes. Therefore we will utilize the remote sensing data and other spectral measured data to retrieval the distribution of the Chl-*a* concentration. Combine with the satellite retrieval results and Duflow water quality model to simulate and predict the dynamic changes of phytoplankton in a certain period.

1.4. Research Questions

The objectives mentioned above, the data are to be collected and methods selected will address the following formulated research questions:

- How to define the relationship between phytoplankton concentration (C_{chla}) and surface reflectance.
- Can the concentration and spatial distribution of phytoplankton (C_{chla}) be assessed by use of SPOT 6 sensor's 4 visible/reflective infrared spectral band with 6 m spatial resolution.
- Can the water flows and phytoplankton concentration of the Kristalbad be simulated using a simplified urban system model approach (e.g. DMS model)?
- Is a DMS model useful to portrait and predict the changes of phytoplankton concentration under certain weather conditions of the Kristalbad?

1.5. Thesis Structure

The thesis is divided into eight chapters:

Chapter 1: The introduction of the overview of the research background. It consists of the other detailed information of the topic, including the research problem, research objectives, and specific research questions.

Chapter 2: In this chapter is the literature review on the research topic. It introduced the research progress in three aspects, review on the wetland aquatic vegetation for nutrients removal; review on remote sensing for deriving Chl-*a* concentration; review on water quality modelling.

Chapter 3: This is mainly introducing the detailed information about the study area—Kristalbad. It make up by three parts: (1) the history and location of the Kristalbad; (2) the scheme of the Kristalbad; (3) the main functions of the Kristalbad.

Chapter 4: The description of the research materials and the method for processing the in-situ data. Research materials are divided in three parts first is the field measurement data, the second is the high-resolution satellite image data, the third is collected from water authority. Field data could be separated in two sets, the one including the field water sampling and field spectra data which are used to develop the empirical model for mapping the Chl-*a* in Kristalbad; the other is the hydraulic and hydrochemical data about the Kristalbad which are used to build the hydraulic water quality model. The high-resolution satellite data (SPOT 6) need to participate in these two processes, after pre-processed to extract the remote sensing reflectance.

Chapter 5: In this chapter is mainly describing the algorithmic method to derive the relationship between the lab-measured chlorophyll-a concentration and the field measured remote sensing reflectance.

Chapter 6: In this part, we are integrating the high resolution remote sensing (Spot 6) with the DUFLOW water quality modelling to detect the behavior of the chlorophyll-a in a mid-long period in Kristalbad. And we'll also test the feasibility to monitor the chlorophyll-a in different weather condition, such as the dry season, wet season, and extreme season.

Chapter 7: The final assessment, involves the laboratory analysis results, the remote sensing reflectance characteristics of the water in Kristalbad, the spatial distribution of the phytoplankton, and the mid-long term behavior of the phytoplankton in Kristalbad.

Chapter 8: The conclusions and the future recommendations of the research. Also the limitations are listed in this chapter.

1.6. Work flow

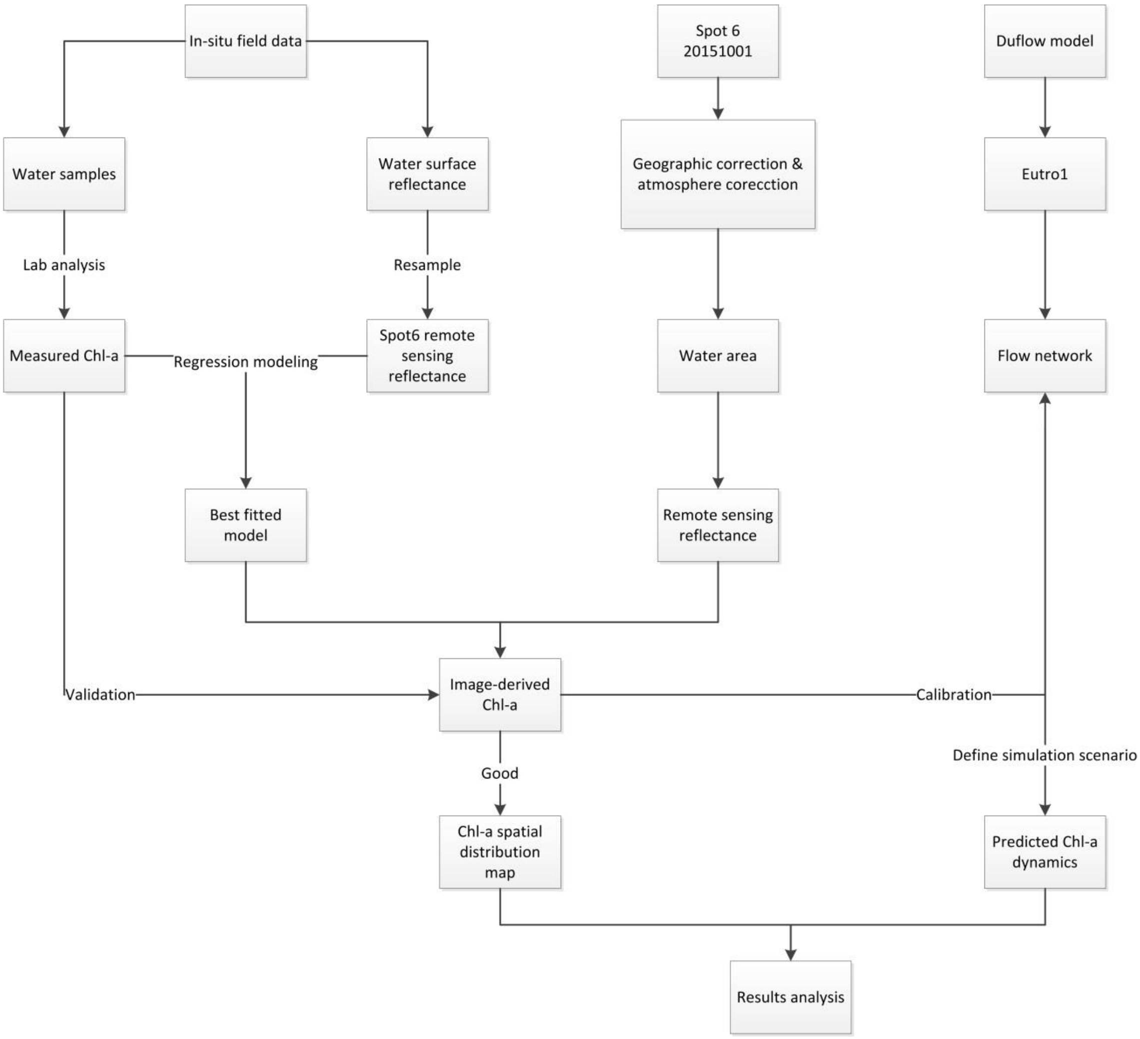

Figure 1-3 Flow chart of research method

2. LITERATURE REVIEW

2.1. Review on wetland aquatic vegetation for nutrients removes

The increasing of the industries, population and human activities lead to increasing demands of using water. This will cause a destruction of water ecosystems and an augmentation of water pollutions. And these are the main sources of nutrient supplements in water environment. When nutrients excess the limitation in a water ecosystem, it will lead to the eutrophication and damage to the public health.(Bissonnette & Skousen, 2001; Iamchaturapatr et al., 2007) There have many ways to remove the nutrients in the aquatic system. One deliberated approach used for effluent (contains high nutrients) purification is utilizing the wetlands (both natural and artificial). Wetlands as biological treatment systems, which contain various aquatic plants and phytoplankton are used for treating the water and purifying polluted water from high nutrients(Iamchaturapatr et al., 2007). At the same time, this method contains biological, physical and chemical three complex processes. Therefore, the wetland aquatic vegetation plays an important role in purifying the urban effluents. The initial function of removing the nutrient loads is through filtering and setting of organic and inorganic particles which associated with the nutrients to make them pass slowly through the wetland. (Nichols, 1983) The aquatic vegetation also as a substrate for attaching the decomposed microorganisms(Jong, 1976; Tóth, 1972), which behave like a filter to block dissolved organic matters. Furthermore, aquatic vegetation influences the nitrification and denitrification by controlling the dissolved oxygen concentration of the wetland within the rhizosphere(ARMSTRONG, 1964). And they also can provide bacteria to fix the N in root nodules(Fisher & Acreman, 2004). All above these give a good evidence to prove a great capability of aquatic vegetation in purifying wastewater.

2.2. Review on remote sensing to derive the Chl-*a* concentration

In traditional, wetlands monitoring has been based on amount of ground surveys and laboratory measurements. However, the results of these field works are general incompatible, due to different surveys extent, sampling intensity and sampling methods. Moreover, it's difficult to dynamic monitor the spatial and temporal variability of the mass of the phytoplankton and aquatic plants, let along to predict a series changes in the wetlands. To address these problems, the remote sensing approach needs to be applied in this research. Remote sensing can provide macroscopically views of monitoring water quality, in particular, the spatial distributions of phytoplankton. (Tyler, Svab, Preston, Présing, & Kovács, 2006)

In general, remote sensing based on surface reflectance (R_{rs}) data are typical to render consistent large scale observations and this can be linked to ecological phenomena.(Liu & Cheng, 2010) in the case of ocean area, the earth observational satellite sensors, such as the Sea-Viewing Wide Field-of-View Sensor (Sea WiFS) have already applied to estimate the C_{chla} (J. E. O'Reilly et al., 1998; Subramaniam, Brown, Hood, Carpenter, & Capone, 2001); the Moderate Resolution Imagining Spectroadiometer (MODIS) can be optimally used to retrieval the C_{chla} in coastal area(Moses, Gitelson, Berdnikov, & Povazhnyy, 2009); the Medium Resolution Imaging Spectrometer (MERIS) is widely used to monitor the water properties in large scale with the wavelength ranges from 390 to 1040 nm(Moses et al., 2009) However, in the small lakes likes Kristalbad, where required the detail spatial resolution (meters), the high spatial resolution sensor such as SPOT 6, Formosat-2 and Landsat 8 make it superior to the low-spatial resolution systems(Chang et al., 2009; Singh, Ghosh, Sharma, & Kumar, 2014; Yang, Sykes, & Merry, 2000).

Using remote sensing to assess Chl-*a* concentration in the water was utilized the chlorophyll-a's spectral properties which absorbs light greatly near (~400 nm) and the minimum absorption near (~550-555 nm) where is the green band. The algorithms which use these properties are applied in ocean firstly, such as the

OC2-OC4. And these algorithms needed to be developed to applied in different types of water through using the empirical, analytical and semi-analytical methods (Gitelson et al., 2008; Kahru & Mitchell, 1999; J. O'Reilly & Maritorena, 2000)

The "empirical model" is very simple and inaugurated by spectral characters of the Chl-*a* in water for varying concentrations. In case Ⅰ ocean water which is clear and considers phytoplankton to be non-water absorption, the empirical algorithm such as the OC4v4 utilize the spectral channels ranges between blue and green to estimate the C_{chla} (Bosc, 2004; J. O'Reilly & Maritorena, 2000) Therefore the empirical model OC2- often used to estimate the C_{chla} between 0-10 mg/m3(Odermatt, Gitelson, Brando, & Schaepman, 2012). However, the spectral channels are not only affected by the C_{chla} , but also by some other water constituents such as the colored dissolved organic matters (CDOM) and suspended matters (SPM). Therefore, for the turbid and productive inland water where the affected by the CDOM and SPM could be negligible, the use of the peak near 700 nm and the reflectance ratio models of R_{rs} max/ R_{rs} (670) to estimate C_{chla} have been applied in many researches(Choe, Lee, & Cheon, 2015; Lim & Choi, 2015; Luoheng & Rundquist, 1997) There have other wavelength ranges, e.g. 430-450, 490-550, 605-620, 690-710, and 826-846 nm, are the most sensitive ranges to the Chlorophyll pigment(Ma & Dai, 2005). The simple two bands ratio between the red (670 nm) and NIR has been widely used, because the NIR directly related to the chlorophyll density and red reflectance inversely related(Luoheng & Rundquist, 1997). But for most high resolution satellite sensor such as Spot 6, formosat-2, they do not have the red-edge range band (near 710 nm), therefore, simple two band ratio between the NIR (710 nm) and Red (670 nm) could not be applied in this research. In the recent researches, the multiband ratios have been proposed and used for estimating C_{chla} , because the algorithms are propitious in retaining the highest satellite sensor signal-to-noise ratio (SNR) for different C_{chla}(J. O'Reilly & Maritorena, 2000). And a Blue-red-NIR model have been developed and successfully applied on the high-resolution satellite data for retrieval of the C_{chla}. In this study, the water of Kristalbad is optical complex and combines the optical properties of the case Ⅰ and case Ⅱ water, due to the field measurement carried out during the winter season, where the runoff, sediment load, phytoplankton blooms could not be observed. Therefore, the water of Kristalbad acts as the case Ⅰ water with moderate C_{chla} during the winter season but during the summer, it behaves like the case Ⅱ water. Therefore, the water in Kristalbad could not be simple deals as the case Ⅱ water for this research. In order to quantify the C_{chla} of Kristalbad, the multiband empirical algorithms are adopted to detect the relationship between bio-optical characteristics and the chlorophyll-a concentrations. All the possible multiband ratios will be tested and apply the best-fit model on the satellite data to map the spatial distribution of the phytoplankton.

2.3. Review on modelling of the Chl-*a* concentration

Although, remote sensing is a well-established tool for quantifying and monitoring the distribution of phytoplankton across temporal and spatial, its application of predicting the phytoplankton blooms has not been so successfully. This is mainly because the phytoplankton blooms are related to the concentration of the nutrients (nitrate, phosphate) in the aquatic system. Many researchers have tried to build a relationship between phytoplankton concentration and nutrients concentration(Anderson, Glibert, & Burkholder, 2002b). But this relation is not a constant and the concentration of nutrients is affected by many factors, temperature, rainfall, runoff, and soil and landuse(Schilling & Zhang, 2004).

Other researchers have attempted to deal with this problem by using the water quality model. For instance, Hamilton and Schladow (1997)use a one-dimensional water quality model (DYRESM Water Quality) combines a hydrodynamic model (DYRESM) to simulate the phytoplankton production, nutrient cycling.

On the other hand, deliberated approaches to dynamic monitor the wetland is using a water quality model —— DUFLOW is applied to simulate the flow movement and constituent transport in open especially for the advection and dispersion of the constituent transport. It is easily to simulate the changes of chlorophyll-a concentration for a time series(Vieira, 1998).

But there is a new idea to utilize the combination of the remote sensing and hydraulic modelling to deal with the prediction problem. It have been proved that, it is possible to integrate the high-resolution remote sensing data and water quality model to determine the behavior of the phytoplankton in a river (Choe et al., 2015). And then with the help of the both remote sensing and modelling it should be possible to analyze the potential of the algae blooms for a mid-long term. This can be used to prevent the hazard of the algae blooms and optimize the ecosystem management.

3. STUDY AREA

This chapter contains information about the Kristalbad. In the following sections, information will be given about the history and location, the design, the water machine and the functions of the Kristalbad.

3.1. History and Location

The Kristalbad was one of the Twente Marken Twekkelo and Driene, and later became the hamlets Twekkelo and Driene. In the nineteenth and twentieth century many changes took place in this area. The Elsbeek was straightened where a sewage treatment plant was built at the Bruggenmorsweg between the urban areas of Enschede and Hengelo.

The origin of the Elsbeek cannot be identified well, probably because there was a connection with the other streams in the north of Enschede. In the area of Kristalbad, stood Cuckoo Beek in Hengelo was this Berflosche beek (Unknown, Map water boards in 1882, 1882 and modified in 1884). Figure 2 shows a map with the situation around 1917.

Figure 3-1 The northern area of Enschede in 1917.

In 1942 a permit was requested from the municipality of Enschede for the construction of a wastewater treatment plant. In 1945 the construction of the wastewater treatment plant was completed, therefore, the effluent was then discharged into the beginning of the Elsbeek. In the sixties, were several things adapted to the Elsbeek one of is a storage area need to be built where now is Kristalbad. Kristalbad is an important project which kook ten years hard work. It will be used to post- treat the effluent from the wastewater treatment plant. Appendix 1 contains a map and incorporated a process diagram of the WWTP Enschede West.

Figure 3-2 shows the location of the WWTP Enschede West, the Elsbeek, the Kristalbad and the rest of the Elsbeek. Northwest of the Kristalbad is the urban area of Hengelo and southeast lies the urban area of Enschede. The municipal boundary between Enschede and Hengelo walk straight through the area. The Kristalbad lies at the point where the city each closest approach. Southwest of Kristalbad is the Twente Canal and the hamlet Twekkelo. To the northeast are the Hengelose- and Enschedesestraat and hamlet Driene.

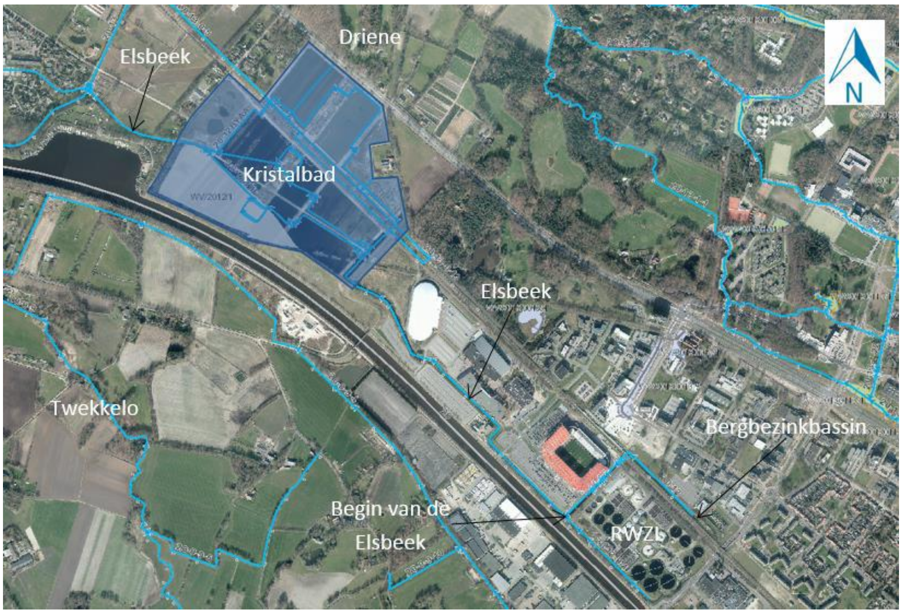

Figure 3-2 The outline area are Twekkelo, Driene, WWTP Enschede, storage settling tank, Elsbeek and Kristalbad. Obtained via geoweb

The railway line Hengelo-Enschede cuts through the area. The water that flows into the Kristalbad coexists with occasional overflows entirely of effluent from the wastewater treatment plant Enschede West. The inlet of effluent from the wastewater treatment plant Enschede West is the beginning of the Elsbeek. At this same point is also an overflow channel from the Elsbeek, this channel is connected to the storage settling tank from the municipality of Enschede in the Auke Vleerstraat. The contaminated water during an overflow of storage settling tank in the Elsbeek flows has only a limited impact on water quality in the Elsbeek, according to recent research.

3.2. The Scheme of Kristalbad

The Figure 4 shows the scheme of the Kristalbad which purifies water from the sewage after. The area consists of three sections. The sections are shallow and have to overgrow in a natural way. The vegetation in these sections will purify the effluents, so Elsbeek will contain more oxygen. The Elsbeek flows into the distribution channel of the Kristalbad in at the southernmost point of the area. The water leaves the Kristalbad along the Hengelose side, and then flows further into the Elsbeek. Between compartments II and III are the railway area and the bicycle highway (F35). The ecological corridor is clearly visible as a green road that crosses the compartments. In the compartment I was still part of the old boundary mark visible (Eelerwoude Veenstra & Abe, 2010). The total area of the Kristalbad is 40 hectares and contains approximately 34.7 hectare of the wet parts.

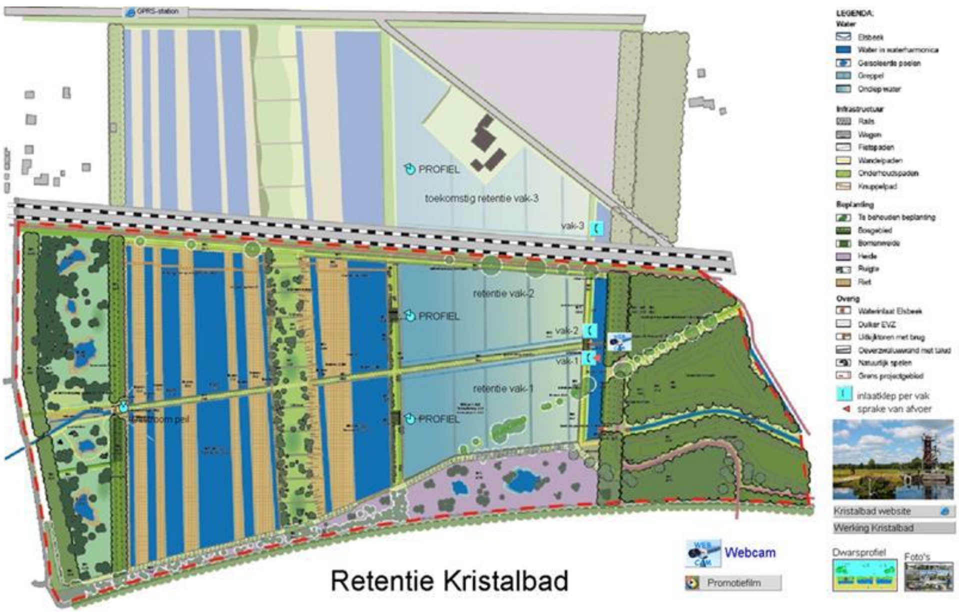

Figure 3-3 The scheme of Kristalbad

In the distribution channel the effluent coming from the Elsbeek distributed over the different compartments. It is expected that most of the sludge to settle out of the effluent in the distribution channel. In the distribution channel contain various aquatic vegetation which use for removing the heavy metals and nutrients from the water.

The water depth varies in the different parts of the Kristalbad. The flood plain is shallow and there as the flood plain filled on average about 0.3 m of water. There is a height difference of about 0.3 m between the beginning and the end of the flood plain. In the wetlands is part 0.50 - 0.80 meters deep while other parts are deeper again. During rainwater supply the water level is about 1.0 - 1.3 m rise. The average water level of the Elsbeek before and after the Kristalbad is approximately 0.4 m. The slope of the flood plain is 1: 1.5. The slope of embankments of the reed bed and wetland is 1: 2. The slope of the distribution channel is slightly less steep, and is 1: 3. In Appendix 2 to find the cross sections of the Kristalbad.

3.3. Functions of Study Area

Kristalbad mainly have four functions and the project objectives were formulated in Figure 3-4, the targets are visible:

- Making space for water retention;
- Improving water quality (chemical and ecological);
- The formation of an ecological connection (EHS);
- Room for recreational use.

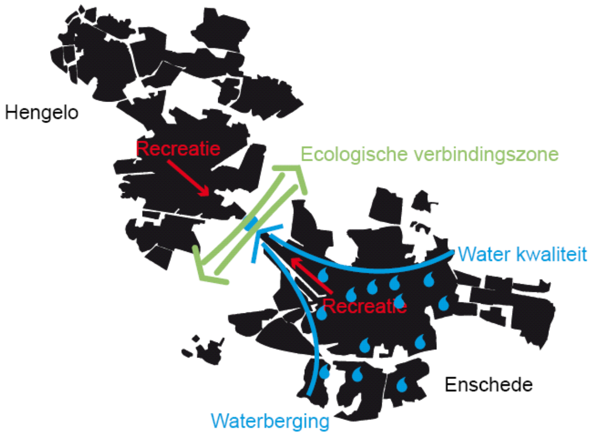

Figure 3-4 The objectives of the various functions for the Kristalbad (van der Wiele P., 2013).

3.3.1. Water retention

Enschede is located partially on a moraine and lateral moraine formed by a glacier or ice sheet, see Figure 3-5. This is a height difference of ± 45 meters in Enschede. During heavy rains, rainwater flows quickly towards Hengelo, causing flooding in low-lying areas in Hengelo (van der Wiele P., 2013). This is because the Elsbeek rainwater from Enschede directly drains into the direction Hengelo. Kristalbad was built as retention between Enschede and Hengelo. In the water retention area is captured temporarily before it is further discharged. In Kristalbad is in addition to the daily volume of 173 500 m^3 of creating a retention volume of 187 000 m^3 to prevent future flooding in low-lying areas.

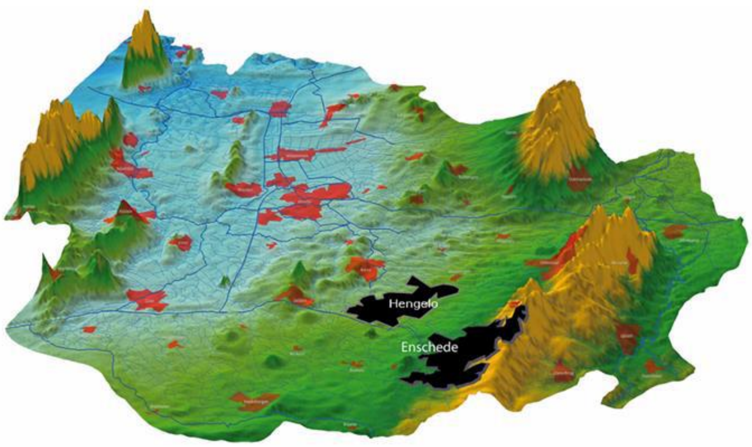

Figure 3-5 Elevation map; Enschede is located on the eastern moraine and Hengelo is located in a lower area (van der Wiele P., 2013).

3.3.2. Water Purification

Purification of the effluent of waste water treatment plant of the Enschede West is a secondary function of the Kristalbad. The water quality in the Elsbeek has always been of poor quality, through the post-treatment of the effluent quality in the Elsbeek will most likely increase. In Elsbeek, the distribution channel, the flood plain, the aquatic vegetation, the wetlands and the spillway where the water flows back into the Elsbeek the different purification processes take place.

3.3.3. Ecological function

The Kristalbad forms an ecological corridor which the former Twente Marken Twekkelo Driene and connect with each other. Between the Kristalbad and Twekkelo hamlet located between the Twente Canal and the Kristalbad and hamlet Driene are the Hengelose- and Enschedesestraat. For the ecological corridor in the Kristalbad was chosen for a dry and wet-dry corridor type (Unknown, Fauna Passages Enschede / Hengelosestraat, 2009). This choice is based on the target species which should be able to make use of the corridor. The target species are pine martevs, bats, the apatura iris, the deer, the white admiral, badger, red light vole, the moor frog and the common lizard.

3.3.4. Recreational function

Recreation is a secondary function of the Kristalbad. More and more people come to the Kristalbad for bicycling or walking. It is possible to take a walk around the Kristalbad, on the way there are information panels, plank bridges and two Towers; one in Enschede and the other in Hengelo. The bicycle highway (F35) cut parallel to the railroad through the area. The route goes along the Enschede Kristalbad (Eelerwoude, 2010). The area is also popular with bird watchers and nature lovers due to a great diversity of birds. So far there are about 160 different bird species spotted in the Kristalbad.

3.4. Temperature

The climate of the Enschede and Hengelo features the oceanic climate (Cfb in the Köppen classification) (Kottek, Grieser, Beck, Rudolf, & Rubel, 2006). Due to its inland location, therefore, the winters are less mild than the rest of the Netherlands. Table 3-1 and Figure 3-7 show the daily temperature data of every month during 1981-2010 at the Twente station. The data collected from Royal Netherlands Meteorological Institute (KNMI). The annual mean temperature is about 3°C during the winter season and is about 16°C during summer.

Table 3-1 Daily temperature of every month from 1981 to 2010. Obtained from web

Temperature data for Twenthe (1981-2010)													
Month	**Jan**	**Feb**	**Mar**	**Apr**	**May**	**Jun**	**Jul**	**Aug**	**Sep**	**Oct**	**Nov**	**Dec**	**Year**
Average high °C	4.8	5.7	9.5	13.9	18.0	20.5	22.8	22.5	18.7	14.1	8.9	5.2 (41.4)	13.72 (56.69)
Daily mean °C	2.3	2.6	5.6	8.9	12.9	15.4	17.6	17.1	14.0	10.2	6.0	2.9	9.63
Average low °C	−0.5	−0.6	1.5	3.4	7.1	9.6	12.0	11.5	9.2	6.2	3.0	0.3	5.23
Source: KNMI													

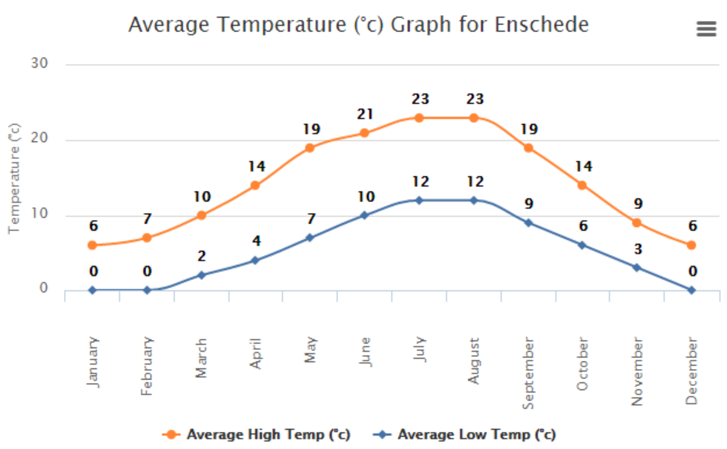

Figure 3-6 Average High/Low Temperature for Enschede, Netherlands. Obtained from wed.

3.5. Precipitation

In the Netherlands, rainfall is distributed averagely in four seasons. During the dry season (January- June), the monthly rainfall is about 40-60 mm; summer season (July - December) is about 60-80 mm/month. Table 3-2 shows the average monthly precipitation (mm) and evaporation of the Twente during 1981-2010. The annual average precipitation and evaporation are about 780 mm and 460 mm, respectively. Figure 8 shows the average rainfall and rainfall days for Enschede.

Table 3-2 Average Monthly rainfall and evaporation of Twente from 1981 to 2010. Obtained from web

Rainfall data for Twenthe (1981-2010)													
Month	**Jan**	**Feb**	**Mar**	**Apr**	**May**	**Jun**	**Jul**	**Aug**	**Sep**	**Oct**	**Nov**	**Dec**	**Year**
Average precipitation (mm)	71.5	51.6	65.1	45.2	62.4	67.7	74.5	71.0	65.4	67.5	68.9	74.1	784.9
ETo (mm)	7.43	14.26	31.22	57.45	83.39	89.57	95.07	78.98	48.66	26.93	10.56	5.89	457.8
Source: KNMI													

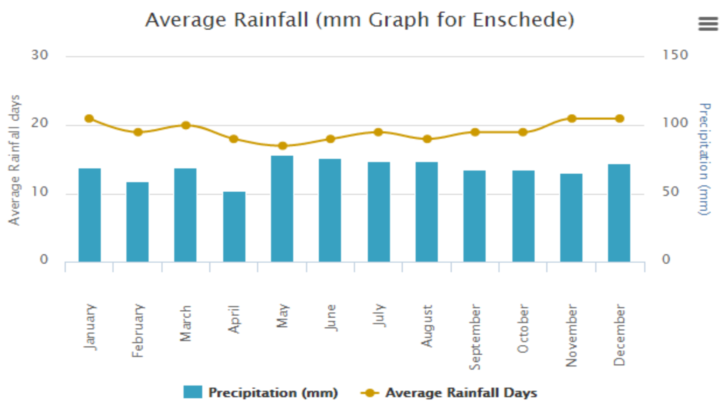

Figure 3-7 Average Rainfall (mm) and rain days ofor Enschede. Obatined from web

4. MATERIALS AND METHOD

This chapter mainly describes the general approach to collect and process the available data in this research. All the available data include the high-resolution satellite data (SPOT 6), spectral measurement data (R_{rs}), field water sampling and other detailed data of the Kristalbad.

4.1. In situ Measurement

4.1.1. Water Sampling

The total 7 water samples were collected in Kristalbad wetland during the winter season, on October 1st, 2015, at the locations below (shown in Figure 4-1). All these samples were taken at less than 0.3 m depth waters along the bank of the pods, immediately after the spectral measurements were made. The time of the field campaign was planned to start during the satellite overpass time (around 10:00 clock) in order to improve the accuracy when linked to the satellite data. The positions of the sample sites were recorded by a hand-held Trimble GPS receiver. The S1 sample and S6 sample were located at the input and output of the Kristalbad, respectively. And the S7 was the sample, which the colour is very different other samples (shows in Figure 4-1). In this research, all the samples have been used for retrieving the concentration of chlorophyll-a through combining the satellite data and spectral measurements using a Trios/Ramses spectrometer.

Figure 4-1 location of sample sites.

4.1.2. Laboratory Analysis of the C_{chla}

The water samples were analysed in the ITC laboratory, on the day after field sampling. Water samples were kept at -20 °C in the dark in the fridge and after filtered via Whatman GF/C filter and analysed for the C_{chla} following the method 446.0: In Vitro Determination of Chlorophylls by Visible Spectrophotometry(Arar, 1997). Chl-*a* pigment was extracted using 90% acetone at 4°C for overnight under dark conditions. In this research, 700 ml filtered water sample and 100 ml extraction solution were required. Also there have 4 ml water sample absorbed by the filter paper.

Measure the sample's absorbance at each wavelength by using the spectrophotometer. Warm up the spectrophotometer (Visible, multiwavelength, with a resolution less than 2 nm) and use the 90% acetone to zero the instrument at all selected wavelengths. To determine the Chl-*a*, the absorbance at the 750 nm, 664 nm, 647 nm and 630 nm are used in the Jeffrey and Humphrey's Trichromatic Equations – Subtract the absorbance value at 750 nm from the absorbance values at 664, 647 and 630 nm. Following equation:

$$C_{E,a} = 11.85(\text{Abs } 664) - 1.54(\text{Abs } 647) - 0.08(\text{Abs } 630) \qquad (1)$$

$C_{E,a}$ = concentration of chlorophyll-a (mg/L) in the extraction solution.

Calculate the total concentration of chlorophyll-a in the water sample using the following general equation:

$$C_{s,a} = \frac{C_{E,a} * extract\ volume\ (L) * DF}{sample\ volum\ (L) * cell\ length\ (cm)} \qquad (2)$$

$C_{s,a}$ = concentration of chlorophyll-a (mg/L) in the water sample.

$extract\ volume$ = volume of extract solution (L) (in this case is 0.0104).

DF = any dilution factors.

$sample\ volum$ = volume of the whole filtered water sample (L) (in this case is 0.07).

$cell\ length$ = optical path length (cm) of cuvette used (typically 1 cm).

In this research, other quality variables as suspended matter, turbidity, temperature were also measured. The entire laboratory analyses were carried out with not less than three replicates.

4.2. Surface reflectance measurements

4.2.1. Collection of the hyperspectral data

Water-leaving reflectance $R_{rs}(\lambda)$ measurement was taken on the same day and same locations with the water sampling (shows in Figure 4-1). In general, the greatest discrepancies of the $R_{rs}(\lambda)$ spectra relative to the TriOS system were mainly due to environmental conditions during data collection. But in this research, on the Oct 1st, 2015 the weather condition is very suitable for spectral measuring, because the wind speed lower than 5 m/s; cloud cover is 1.7% and clear on the study area; the sun angle is high. At each sampling site, the surface reflectance $R_{rs}(\lambda)$ measurements were carried out using the TriOS Ramses radiometers. This radiometric measurement system consists of three TriOS Ramses hyper spectral radiometers which could measure spectral properties at the detailed wavelength ranges from 350 to 950 nm (Figure 4-2 shows the measurement with TriOS Ramses). And it has a various spectral resolution from 3.26 to 3.35 nm.

Figure 4-2 Spectral measurement with TriOS Ramses spectrometer.

To obtain the water- leaving reflectance $R_{rs}(\lambda)$ is to compute the ratio between the total upwelling above water radiance and total downwelling radiance. The method of measuring $R_{rs}(\lambda)$ we followed the procedure described by previous researches (Lee et al., 1998; Mobley, 1999). Three parameters should be measured: (1) the total downwelling irradiance $E_d(\lambda)$; (2) the downwelling radiance from the sky $L_{sky}(\lambda)$ was measured with radiometer looking upward at 42 deg from zenith; (3) the total upwelling radiance $L_u(\lambda)$ at 42 deg from nadir and an azimuth angle at 138 deg. All these angles are adopted from the previous studies(Mobley, 1999).

4.2.2. Data processing

The water-leaving radiance $L_w(\lambda)$ which measured at an angle of 42 deg from nadir and an azimuth angle at 138 deg, it can be calculated following the equation (3).

$$L_w(\lambda) = L_u(\lambda) - \rho * L_{sky}(\lambda). \tag{3}$$

In Eq. (2), ρ is the air–sea interface reflection coefficient, which is dependent on the wind speed (W) in m s^{-1}. Mobley *et.al* recommended that when wind speed was not measured or lower than 5 m s^{-1}, the value of ρ equal to 0.028 is acceptable.

Subsequently, the water-leaving reflectance $R_{rs}(\lambda)$, at θ = 42 deg relative to the zenith, is derived following the equation (4).

$$R_{rs}(\lambda) = \frac{L_w(\lambda)}{E_d(\lambda)} \tag{4}$$

4.3. Remote Sensing Data

4.3.1. Satellite for Observation of Earth (SPOT 6)

The SPOT 6 is a commercial high-resolution optical imaging Earth observation satellite system operating from space. The Spot 6 imagery has the 2 m resolution in panchromatic (PAN) and 6 m resolution in the multispectral (MS) bands. Spot 6 contains four spectral bands from 450 to 890 nm wavelength including the blue, green, red and near-infrared. The scene coverage of the Spot 6 is 60 x 60 km. Table 4-1 shows the spectral specifications and resolution of Spot 6. Spot 6 not only offers the high spatial but also the temporal resolution, since they can revisit a same area, every day with a constant viewing angle. This sensor generation characterized by repetitive acquisitions of high resolution images is very useful for monitoring land surface dynamics(Courault et al., 2008).The image shown in Figure 4-3 was acquired on 1st October 2015 in relation to the date of field campaign.

Table 4-1 Spectral specifications and spatial resolution

Band number	Spectral range(μm)	Spatial resolution(m)
Band 1	0.45-0.52	6
Band 2	0.52-0.6	6
Band 3	0.63-0.69	6
Band 4	0.76-0.9	6
PAN	0.45-0.9	2

Figure 4-3 Spot 6 image of Kristalbad acquired on 1st October 2015

4.3.2. Data processing

The Spot 6 image was orthorectified using the Digital Elevation Model (DEM) and its Rational Polynomial Coefficient (RPC) operated through the ERDAS IMAGINE (the image processing and GIS software package). Orthorectification is the process of removing distortion in the image. The Spot 6 image will also be used to provide the detailed background information of the Kristalbad which help to build the DMS model. Then the water body of the Kristalbad was identified by the unsupervised classification which classified the near infrared band (band 4) of Spot 6 into two categories – water area and non-water area through the ERDAS IMAGINE. Using recode module to renumber the classes, the water area set to "1" and other classes to "0". Then extract the water by using the mask module in ERDAS. This step was performed to pick water areas on the image and minimize the effect of land, vegetation, or man-made structures on image analysis. The water area of Kristalbad is shown in Figure 4-4.

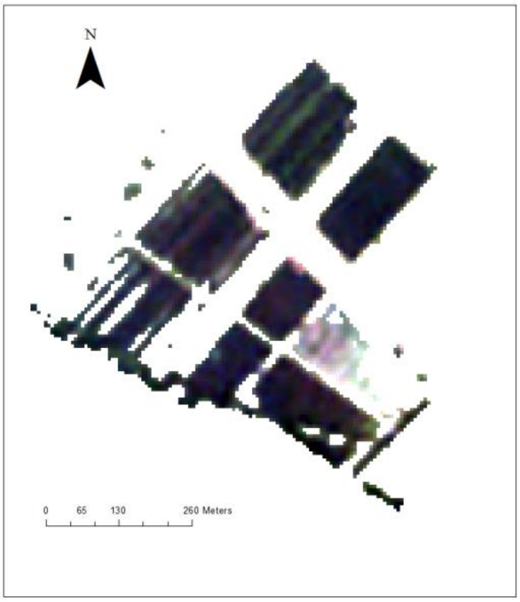

Figure 4-4 Water area of Kristalbad

4.3.3. Atmospheric correction

In order to quantitative of remote sensing, an appropriate atmospheric correction method needs to be applied to convert the DN value of image pixels into remote sensing reflectance from radiance. For high resolution imaging data, there are a number of atmospheric correction algorithms have been developed, such as the Atmosphere CORrectioN (ACORN), the Imaging Spectrometer Data Analysis System (ISDAS), the High-accuracy Atmospheric Correction for Hyperspectral Data (HATCH). In this case, the Fast Line- of-sight Atmospheric Analysis of Spectral Hypercube (FLAASH) was applied on the Spot 6 atmospheric correction. FLAASH is based on an atmospheric radiative transfer model, Moderate Resolution Atmospheric Transmission (MODTRAN 5). The atmospheric correction was operated in ENVI software.

4.3.4. Match the field sampling sites with the SPOT pixels

For retrieval of the Chl-*a* concentrations from the satellite image, the first step is to matched sample locations to the specific pixels on the image. One corresponding pixel was matched with one sample site, not apply the window method to average the pixel (3x3, 5x5, etc.). Because Kristalbad is very small, and sampling stations are interfered by many things, such as weirs, vegetation on the bank, and their shadows, therefore the pixel value can be affected when the image is applied an automatically averaged n x n windows. The total sample sites and linked pixel reflectance values are shown in Table 4-2.

Table 4-2 Samples pixel reflectance values

Sample code	Pixel reflectance values			
	Band 1	Band 2	Band 3	Band 4
SK1	0.093	0.095	0.04	0.075
SK2	0.095	0.103	0.046	0.048
SK3	0.093	0.096	0.04	0.038
SK4	0.097	0.117	0.049	0.073
SK5	0.092	0.108	0.042	0.08
SK6	0.095	0.134	0.045	0.057
SK7	0.133	0.213	0.037	0.033

4.4. GIS data

GIS data (Figure 4-5) is the geospatial data which is used to identify the detailed geo-information of the Kristalbad, including the coordinates of the inlet, outlet of the Kristalbad and also the water sampling stations. Moreover, the entire network of the Kristalbad was built based on the GIS data and combined with the Spot 6 data as the background. The detailed information including (1) flow section lengths, width, and depth were obtained from the geospatial data and RS data; (2)the cross sections sere acquired by field campaign and previous research; (3) some hydraulic structure also collected from the GIS data, and all of these will adopted in the Duflow modelling.

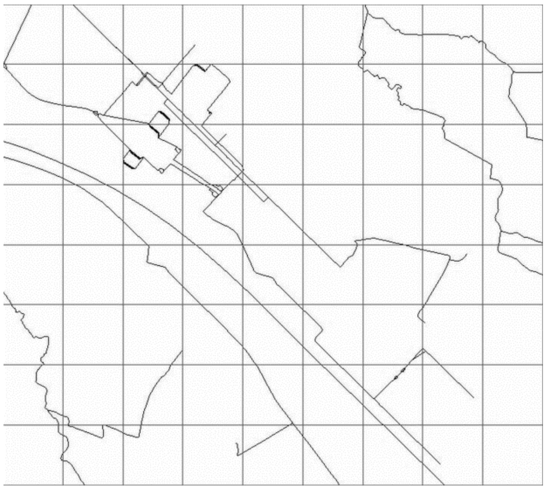

Figure 4-5 Geospatial data of the Kristalbad

4.5. Data Collection from water authority

The data which was collected from Kristalbad was basically used for set-up of the models. In this case, it is mainly used for reasoning out the physical process in the catchment system. The collected data helps to:

- Define model input variables
- Define model parameters
- Assess the process accuracy
- Verify the results

4.5.1. Stream section details

The stream section details are crucial information to define the simulated stream in Duflow. In this research, we assume all stream sections are of the same shapes and size between two nodes, the cross sections structure information must be known. These data obtained from water authority.

4.5.2. Other available data

Some parameters in the water of the Kristalbad are needed, including the water flow parameters (discharge, temperature, etc.), water components (concentrations of NH_4, PO_4, BOD, etc.), and some other external variables (water surface intensity, etc.), all these necessary data are acquired from the local water authority and previous researches(Borg, n.d.).

5. REGRESSION MODELLING

In this chapter is mainly describing the algorithmic method to retrieval the spatial distribution of Chl-*a* concentration from the Spot 6 satellite image by integrating the water-leaving reflectance and in situ Chl-*a*. In order to develop a reliable regression model, two data sets are needed; one is for regression modelling, the other is for model validation. The first set that was used to derive the relationship between the in situ Chl-*a* concentration (C_{chla}) and water-leaving reflectance $R_{rs}(\lambda)$ obtained from the radiometer. Then apply the mathematical relationship on the Spot 6 image to derive the C_{chla} spatial distribution of the Kristalbad. This method skilfully correlated field spectra reflectance with the remote sensing reflectance which obtained from atmospheric corrected satellite image.

5.1. Resampling of hyperspectral data

The $R_{rs}(\lambda)$ hyperspectral data measured with TriOS Ramses radiometer have recorded as 172 bands in the visible band range from 380 to 950 nm, with a various spectra resolution from 2.6 to 3.5 nm. All these $R_{rs}(\lambda)$ hyperspectral data were resampled to four Spot 4 spectral bands $R_{rs}(i)$, including blue band (455- 524 nm), green band (530-590 nm), red band (625-695 nm) and near-infrared band (760-890 nm). The resampled method need to relate to the transmittance functions of the Remote Sensing Imager (RSI) on-board Spot 6. Following the equation (5) is the resample function(Chang et al., 2009).

$$R_{rs}(i) = \sum_{\lambda=400}^{\lambda=1000} R_{rs}(\lambda)T_i(\lambda) \qquad (5)$$

Where $R_{rs}(i)$ is regarded as the remote sensing reflectance obtained by the RSI; i represents the blue, green, red and near-infrared band with the value of 1, 2, 3 and 4, respectively. $T_i(\lambda)$ was given from 400 nm to 1000 nm at 1 nm intervals, based on the pre-launch data. Figure 5-1 shows the spectral sensitivity of Spot 6 satellite acquired form Airbus Defence&Space.

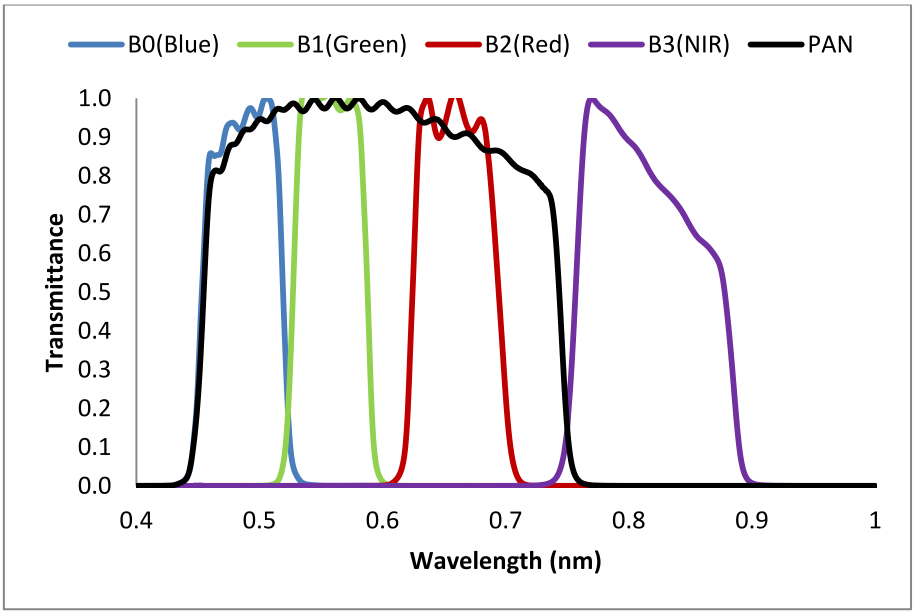

Figure 5-1 Spectral sensitivity for all bands of Spot 6

Table 5-1 shows the result of resampling the TriOS Ramses water-leaving reflectance $R_{rs}(\lambda)$ into four bands of Spot 6 $R_{rs}(i)$ for each sample station. In general, resampled hyperspectral data could retain the most of the spectral features linked to the optical properties of different water types. For this instance the green to blue band ratio and the near-infrared band to red band both are proportional to the concentration of the Chl-*a*, but the accuracy of these methods will be mentioned latter.

Table 5-1 Remote sensing reflectance $\boldsymbol{R_{rs}(i)}$ for each sample station.

Sample code	$R_{rs}(1)$	$R_{rs}(2)$	$R_{rs}(3)$	$R_{rs}(4)$
SK1	0.145	0.162	0.046	0.076
SK2	0.106	0.110	0.048	0.029
SK3	0.129	0.159	0.047	0.053
SK4	0.110	0.170	0.046	0.063
SK5	0.151	0.231	0.053	0.068
SK6	0.073	0.128	0.039	0.082
SK7	0.902	1.421	0.060	0.026

5.2. Water-leaving reflectance and Chl-*a* concentration

In nature, the water-leaving reflectance $R_{rs}(\lambda)$ from a lake is affected by all components of the water body. Due to Kristalbad is a very shallow wetland, therefore, the bottom also could contribute to the water-leaving reflectance $R_{rs}(\lambda)$. To determine which part of the spectral signal is attribute to the chlorophyll-a along is necessary. Retrieving the Chl-*a* concentration from spectral reflectance, the Chl-*a* optical properties could be as the spectral information. The absorption of blue and red light could be as an indicator of the presence of chlorophyll-a pigment. And the maximum reflectance is at the green (560-570 nm) and red-edge (near the 710 nm) also can be taken considered of. In this research, we developed empirical band ratios regression model to retrieve Chl-*a* concentration, because the ratios could enhance latent information when an inverse relationship exists between the spectral responses to the same biophysical phenomenon (Campbell, 2002).

The multiband ratios have been proposed and used for estimating C_{chla}, because the algorithms are propitious in retaining the highest satellite sensor signal-to-noise ratio (SNR) for different C_{chla} (J. O'Reilly & Maritorena, 2000). And a three band ratio between blue (482 nm), red (660 nm) and NIR (825 nm) could be used to retrieval the chlorophyll-a in a very shallow and turbid lake (Singh et al., 2014). The specific objective of this paper is to test the feasibility of multiband ratio, then find a best-fitted model for retrieval chlorophyll-a. All the models tested in this research are referenced the previous research conducted by Singh et al(2014) .At the same time, we will test the performance of the resampled water-leaving reflectance in the regression analysis of the Chl-*a*. These models can be calculated as following equations:

Two-band model: $$C_{chla} \infty \; R_{rs}^{-1}(\lambda_1) * R_{rs}(\lambda_3) \quad (6)$$

Three-band model: $$\mathrm{C_{chla}} \infty \; [\mathrm{R_{rs}^{-1}}(\lambda_1) - [\mathrm{R_{rs}^{-1}}(\lambda_2)] * \mathrm{R_{rs}}(\lambda_3) \quad (7)$$

Where $\lambda_1 =$ 660 nm, $\lambda_2 =$ 485 nm, and $\lambda_3 =$ 825 nm. In this research $R_{rs}(\lambda_1)$, $R_{rs}(\lambda_2)$, and $R_{rs}(\lambda_3)$ are blue, red, and NIR range, respectively, for resampled water-leaving reflectance and Spot6 image bands are 3,1, and 4. Therefore the relationship between measured Chl-*a* concentration and spectral ratio were calculated by all possible linear and non-linear functional forms of regression analysis, such as exponential, polynomial, logarithmic, and power. And the performances of equations used to retrieve the Chl-*a* from Spot 6 image were assessed by the determination coefficient (R^2), root mean square error (RMSE), and relative percentage difference (PRD).The relative percentage (PRD) was used to quantify the absolute difference between imagery-derived and the corresponding observation. The calculation of RMSE and PRD are defined as following:

$$\mathrm{RMSE} = \sqrt{\frac{\sum_{i=1}^{n}(y_i - y_i')^2}{n-1}} \qquad (8)$$

Where n is the number of water samples; y' is the imager-derived values; y is the in-situ measured values.

$$\mathrm{PRD} = \frac{SDV}{RMSE} \qquad (9)$$

Where *SDV* represents the standard deviation of the in-situ measured values.

6. HYDRAULIC MODELLING

In order to understand the behaviour of the Chl-*a* in Kristalbad, we are integrating the high resolution remote sensing (Spot 6) with the water quality modelling on monitoring the changes of concentrations of Chl-a. Remote sensing data used in calibration step to assess the feasibility of its application in water quality modelling. Ultimately, we will used the calibrated the model to predict the changes of Chl-*a* in the future month, from 1st October to the 1st November.

6.1. Duflow description

This study used the Dutch modelling system DUFLOW (version 3.8) for the water quality modelling. This software is very suitable for steady flow and for alternating flow, such as the wetlands. The model package is based on the one-dimensional partial differential equation that describes non-stationary flow in open channels(Abbott, 1979), including the hydraulic flow module, one dimensional equation, water quality module, and a module for groundwater exchange. In this research, in order to simulate the Chl-*a* concentrations in the Kristalbad, the hydraulic module and the water quality module were adapted.

6.2. Water quality modelling—EUTRO 1

The quality model of the Duflow follows a basic 1-D transport equation which illustrates the concentration of a constituent in a 1-D system as function of time and space. For modelling the constituent of Chl-*a* the eutrophication model (EUTRO1) was used in this research, which also describes the effects of nitrogen, phosphorus and oxygen (Figure 6-1). This module can be used to study the short period behaviours of the water system, such as the effects of flushing on the Chl-*a* concentration(Vieira, 1998).

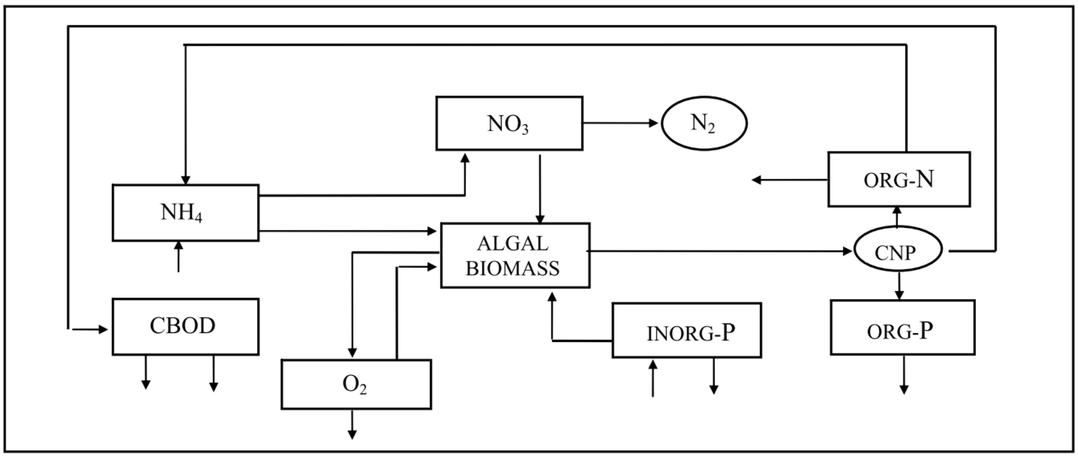

Figure 6-1 EUTRO1 model state variable interactions **(ICIM, 1992)**

The growth of phytoplankton is affected by the environmental condition in Kristalbad, including the nutrients load, surface light intensity, and the water temperature. In this research, we assumed that the phytoplankton could directly use the nitrate and ammonia for their growth. The following equations are describing the process of the dynamic changes of the phytoplankton.

Phytoplankton:
$$\frac{dA}{dt} = [\mu_{max} F_T F_N F_l]\text{A} - [k_{res}\theta_{ra}^{(T-20)} + k_{die}]\text{A} \quad (10)$$

Nutrient limitation:
$$F_N = \left[\frac{P_{ortho}}{P_{ortho} + K_r}\right], [\frac{NH_4 + NO_3}{(NH_4 + NO_3) + K_N}] \quad (11)$$

Light limitation:
$$F_L = \frac{e}{\varepsilon_{tot} Z}[\exp\left(-\frac{I_0}{I_s}\exp(-\varepsilon_{tot}Z)\right) - \exp(-\frac{I_0}{I_s})] \quad (12)$$

Temperature limitation:
$$F_T = \theta_{ga}^{(T-20)} \quad (13)$$

Where:

Input:

A	Algal Biomass	mg C/L
P_{org}	Organic Phosphorus	mg P/L
P_{inorg}	Inorganic Phosphorus	mg P/L
N_{org}	Organic Nitrogen	mg N/L
BOD	Carbon 5 day Biochemical Oxygen Demand	mg O_2/L
NH_4	Ammonia Nitrogen	mg N/L
NO_3	Nitrate Nitrogen	mg N/L
O_2	Oxygen	mg O_2/L

Parameters: The model parameters are used in the EUTRO1 is given in at the end of Appendix 3.

Output:

N_{tot}	Total Phosphorus	mg N/L
P_{tot}	Total Nitrogen	Mg P/L
$Chl -$ a	Chlorophyll-a	g/L

In the phytoplankton balance equation, two terms describing the loss processes, the first one describes the endogenous respiration, which is related to the temperature; the second is a lumped rate constant including the death rate and grazing. Therefore, the phytoplankton activity is significant sensitive to the water temperature and light energy.

6.3. Flow network

The very simplified water system of the Kristalbad was built on a GIS-referenced flow work (Figure 6-2). The Kristalbad have three ponds, the bottom to top is pond 1, pond 2, and pond. In this research, we assume that the start node is the Elsbeek River before flow into the Kristalbad, then the river flows into three tributaries, and each pond could be seen as a tributary, ultimately, these tributaries will flow back into the Elsbeek (the end node). For each pond have three sections, each section have and between two sections connected with structures (weirs and culverts).

Kristalbad was divided into 16 reaches and 38 computational elements. Hydraulic parameters including the time-dependent surface water boundary discharges, water levels, and concentrations for each reach are required form the literatures and field campaign. For this research the actual sill level for weirs need to be added to the model. The division of reaches represents adjoining sections of the flow with same hydraulic and chemical characteristics. Once the initial conditions and environmental parameters have been defined, the DUFLOW calculates the transportation and interactions of the pollutants, and ultimately predicts the changes in Chl-a as well as algal, nutrients for a given time.

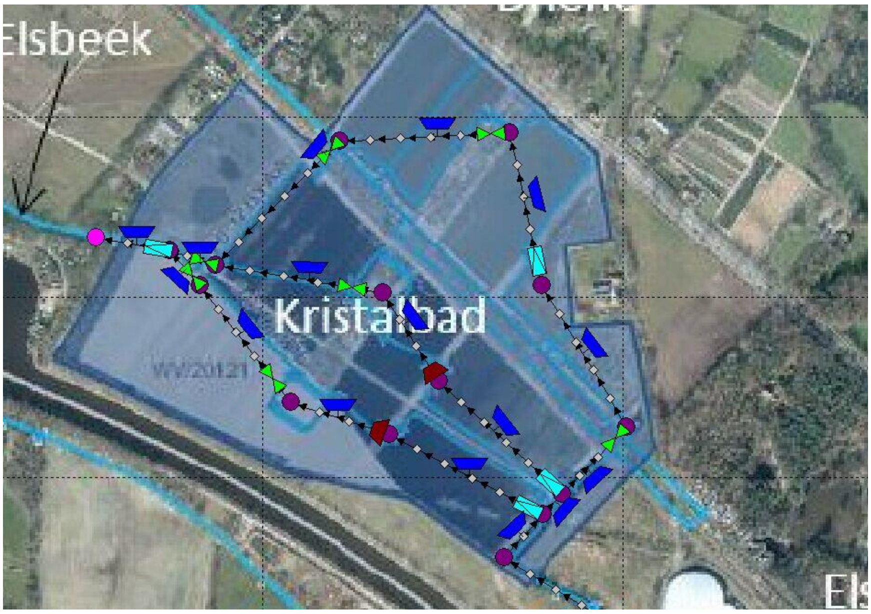

Figure 6-2 Sector of the modelled flow network of the Kristalbad with hydraulic structures.

6.4. Model calibration

Calibration of the model is the procedure to compare the measured data with simulated model results. In this research, the Eutro 1 model was calibrated for chlorophyll-a using data obtained from the Spot 6 imagery-derived datasets. The imagery- derived data were selected at 7 nodes (except the start and end nodes) in the Kristalbad. In these points, the Chl-a concentrations data were used the average value for each sections in each ponds. The adopted calibrated model parameters (Table 6-1)set in the default ranges stated in the similar studies (Vieira, 1998)and a chlorophyll-a to carbon ratio of 30 μg Chl-a/ mg C was adopted.

Table 6-1 Adopted calibrated model Parameters

Parameters	Description	Value	Dimension
μ_{max}	Unlimited algal growth rate	4.0	d^{-1}
K_N	Monod constant Nitrogen	0.01	mg N/L
K_P	Monod constant Phosphorus	0.005	mg P/L
K_{res}	Respiration rate constant	0.1	d^{-1}
K_{die}	Die rate constant	0.2	d^{-1}
I_s	Optimal Light Intensity	40	$W.m^{-2}$
ε_0	Background extinction	1.0	m^{-1}

6.5. Simulated scenarios

After model calibration, we need to define the water condition that need to be simulated. Due to the date we designed the research was during the dry season in the Netherlands, therefore, the simulated scenario should consider the research time, the scenario worked out is summarized in table 6-2. In the table, (1) an average flow discharge and water level for dry season are considered; (2) the variations of phytoplankton limitation factors (light energy, water temperature) are considered. The light energy and water temperature are time series data which adopted daily mean hourly value acquired from KNMI during the 1st October 2015 to 1st November 2015. The time series data is shown in Appendix 4. In this short term analysis, different parts of the Kristalbad —pond 1, pond 2, pond 3 —were considered to display the phytoplankton growth dynamics.

Table 6-2 Simulated scenario

	Water Temperature (°C)	Light Energy (w.m^{-2})	Start node discharge (m3 s^{-1})	End node water level m
Max	18.6	636.64	-	-
Min	0.6	0		
Mean	9.3	42.97	0.8	0.5

7. RESULTS

7.1. Laboratory analytical Chl-a

The concentration of $\mathrm{Chl\!-a}$ at 7 sampling stations ranged from 114.17 to 502.54 mg m^{-3} on the 1st October 2015. And the mean level of the Chl-*a* is over 100 mg m^{-3}. SK1 and SK6 are located at the inlet and outlet of the Kristalbad. The SK7 is the obvious colour and turbid water sample, therefore the concentration of pigments is very high with 502.54 mg m^{-3} chlorophyll-a. The temperature, suspended matters, turbidity and measured C_{chla} are described in Table 7-1.

Table 7-1 Laboratory analysis results of water quality for each sample station

Sample code	Geographic location		Time	Temp. (°c)	Turbidity (NTU)	Laboratory-measured Cchla (mg/m3)	Laboratory-measured SPM (mg/l)
	X(m)	Y(m)					
SK1	351681.75	5790262.84	11:21:03	11	1.94	147.9696237	6
SK2	351541.69	5790540.77	11:50:55	11.1	2.26	187.9381474	12
SK3	351524.65	5790553.74	12:04:29	11.3	2.272	257.0340745	22
SK4	351467.87	5790614.26	12:23:00	11.4	2.686	143.836833	14
SK5	351447.68	5790639.58	12:36:31	11.4	1.7346	114.1708211	16
SK6	351225.6	5790600.06	13:00:54	12	1.632	120.5062857	22
SK7	351141.52	5790564.23	13:23:00	13.5	5.365	502.5392855	No data

7.2. Remote sensing reflectance properties

After resampled the in-situ water-leaving reflectance $R_{rs}(\lambda)$ to four Spot 4 spectral bands $R_{rs}(i)$ and the reflectance values were mostly below 0.25 except the sample SK7. Spectral features of the resamples reflectance was figured out in response to the Chl-a concentration of water samples. In figure 7-1, the four-band spectral reflectance with varying phytoplankton Chl-a concentrations for each sample site showed a reflection peak at green band, an absorption peak at red band, a minor reflectance at NIR band, and a minor absorption at the blue band, these features are roughly similar to the result obtained from previous research by Singh et al.(2014). In the blue region, it was not showed a observious absorpition, this may affected by the reflection by the unsuspended particals and bottom. The maximum reflection at green band (around 560 nm), which related to the absorpition by the phytoplankton chlorophyll and affection by the organic dissolved matters. And the variation is significant in the green band, this phenomenon is linked to the concnetration chlorophyll-a, the high level of the concentration will lead to the high reflection.The low reflection region apperar in the red and NIR band, and this is mainly because the maximum absorption by the phytoplankton chlorophyll. Therefore, the blue-red-NIR three band model could be used to linked the spectral features to the varying chlorophyll-a concentrations.

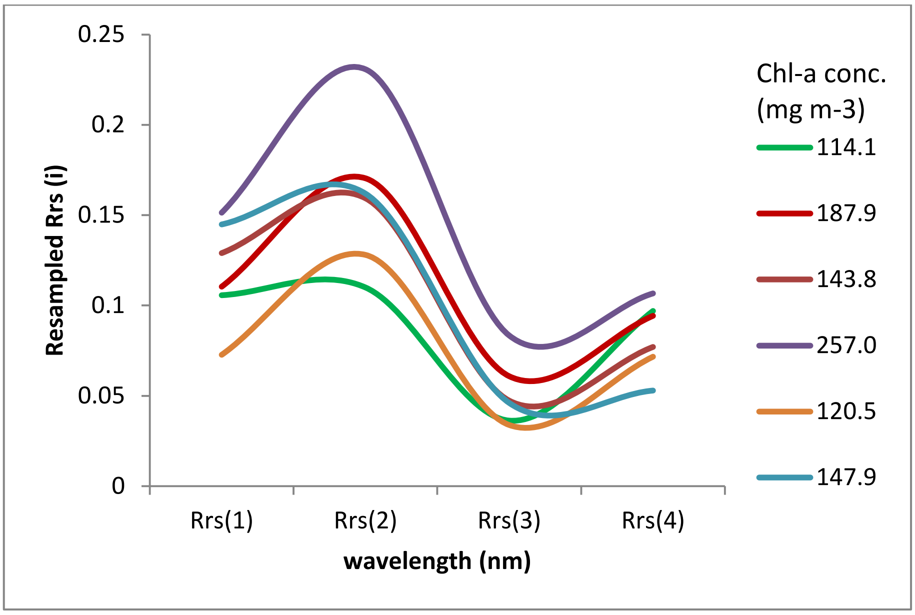

Figure 7-1 Four Spot 6 bands spectral reflectance of resampled $\boldsymbol{R_{rs}(\lambda)}$ with varying phytoplankton Chl-a concentrations for each sample station.

7.3. Chl-a estimation algorithm

All the possible relationships between measured chlorophyll-a concentrations and multiband ratios are calculated by regression analysis. The performances of the each equation fitted with all possible linear and no-linear forms, including linear, exponential, logarithmic, power, and polynomial, and compared in terms of R^2 values. Results are shown in table 7-2.

In this research, we found the linear function of three-band model using blue (485 nm), red (660), and NIR (825) showed significant sensitive to the varying measured chlorophyll-*a* concentrations (Figure 7-2). The equation as following:

Three-band model: $$[R_{rs}^{-1}(660) * R_{rs}^{-1}(485)] * R_{rs}^{-1}(825) \qquad (10)$$

$$Chl\text{–}a = 0.7816(\mathrm{x}) - 7.972 \qquad (11)$$

The best-fitted linear function of the three –band model produced the highest determination coefficient, and the lowest estimation error, and approximate prediction results (R^2=0.84, RMSE = 23.4 mg m- *chl-a*, RPD = 1.39). The research operated by the previous research which firstly used the blue-red-NIR model also showed a high sensitive to retrieval the chlorophyll-a in a productive water(Singh et al., 2014). The model is using the remote sensing reflectance values located in blue (482 nm), red (660 nm), and NIR (825 nm), which are obtained from a high-resolution image data ETM+. In this research, we adopted the reflectance values located in blue (485 nm), red (660 nm), and NIR (825 nm) owing to the position of SPOT 6 image bands, and the values are acquired from resampled filed spectral data. Although the remote sensing reflectance is obtained from different source, but its results is quite similar and can be applied on the SPOT 6 to estimate the chl-a distribution in the space.

Table 7-2 Results of two-band ratio regression modelling show the functional relationship between the R_{rs} and C_{chla}

band ratio	Model equation	R^2
$[R_{rs}^{-1}(660) * R_{rs}^{-1}(485)] * R_{rs}^{-1}(825)$	$y = 0.7816(x) - 7.972$	0.85
	$y = 0.986X^{10.9477}$	0.81
	$y = 244.2\ln(x) - 1136.7$	0.77
	$y = 81.199e^{0.0029x}$	0.82
	$y = 0.0015(x^2) - 0.3202x + 152.51$	0.83
$R_{rs}(485)/R_{rs}(660)$	$y = 14.253(x) + 125.88$	0.75
	$y = 99.935X^{0.4878}$	0.72
	$y = 140.71\ln(x) + 34.66$	0.79
	$y = 137.32e^{0.0491x}$	0.72
	$y = -0.0632(x^2) + 16.079x + 121.69$	0.73
$R_{rs}^{-1}(660) * R_{rs}^{-1}(825)$	$y = -151.43(x) - 392.43$	0.36
	$y = 193.82X^{0.666}$	0.43
	$y = -180.1\ln(x) + 224.8$	0.46
	$y = 371.55e^{-0.586x}$	0.38
	$y = 129.83(x^2) - 478.46x + 564.4$	0.46
$[R_{rs}(485) - R_{rs}(660)]/R_{rs}(825)$	$y = 157.99(x) - 323.36$	0.69
	$y = 156.25X^{0.6137}$	0.49
	$y = 152.34\ln(x) + 170.15$	0.43
	$y = 75.006e^{0.6056x}$	0.70
	$y = 101.67(x^2) - 162.87x + 183.81$	0.77
$[R_{rs}(485) - R_{rs}(660)]/[R_{rs}(485) + R_{rs}(660)]$	$y = 609.59(x) - 91.995$	0.8
	$y = 448.58X^{1.1765}$	0.62
	$y = 332.76\ln(x) + 462.81$	0.71
	$y = 63.928e^{2.1286x}$	0.69
	$y = 997.86(x^2) - 639.95x + 252.84$	0.79
$[R_{rs}^{-1}(660) * R_{rs}^{-1}(825)] * R_{rs}(485)$	$y = 142.73(x) - 77.466$	0.65
	$y = 102.62X^{0.9024}$	0.38
	$y = 269.37\ln(x) + 36.485$	0.49
	$y = 69.654e^{0.481x}$	0.5
	$y = 109.68(x^2) - -375.36x + 466.75$	0.78

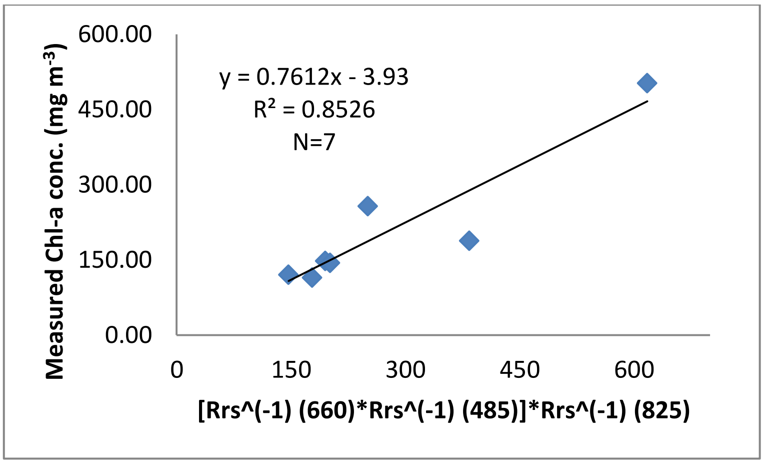

Figure 7-2 Relationship between measured Chl-a and a three-band model with the estimation equation, determination coefficient (R^2), and the number of samples (N).

1.1 The accuracy assessment of the SPOT 6 Chl-*a* mapping

Best-fitted three-band model (eq. (11)) was applied in SPOT 6 image for mapping Chl-*a* spatial distribution showed in figure 16. This calculation procedure was operated by the ERDAS (model maker module). From the Chl-a image, the water area displayed a different level of Chl-a concentration, the bank of the ponds shows a higher level (higher than 200 mg m^{-3}) than the center (lower than 88 mg m^{-3}). In this study, Kristalbad is an optical shallow wetland and most of the water samples are taken close to the bank of the ponds, therefore, the total remote sensing reflectance obtained from the Spot 6 could be contaminated by the vegetation on the bank, shadow, and bottom, and lead to the inversion results are not accurate. In the most researches which using the empirical algorithm to estimate the C_{chla} will remove the bottom albedo from the satellite image, but it cost too much. In this case, the influence by the bottom still exists, but the level of Chl-a concentration is approximately similar to the measured results. Therefore, image derived results are as a guiding analytical tool to provide information covering the entire study area and help to make policies, even a lower accuracy than the measured data (Figure 7-3).

Figure 7-3 Map of Chl-a derived from Spot 6 image taken on the 1st October 2015

In this research, the field measurement was taken during the Spot 6 overpass time. The accuracy assessment was made through comparing the image-derived Chl-a concentrations and in situ measure Chl-*a* concentrations (Figure 7-4), which were matched by coordinates recorded by the GPS. The accuracy assessment has been applied in the total of 7 samples of imagery-derived and laboratory-measured of the Chl-a, through calculation the difference (Δ), root mean square error (RMSE), and relative percentage deviation (RPD) as shown in table 7-3. In the table the difference is high for the last sample, possible due to influence by some other accessory pigments which could affect the absorption measurement in this area. The overall RMSE for the inversion is 31.3 mg m^{-3} and the RPD is 4.39. The correction between the imagery-derived data and the laboratory-measured data were good (R^2=0.88) and the comparison between the data sets were relative close to the 1:1 diagonal line as shown in Figure 7-5. But the differences still exist in this research, because some uncertain factors are included.

In this research, the differences between the measured and imagery-derived C_{chla} are influenced by (1) the strong absorption by the red region will greatly reduce the signal to the sensor and this will affect the SNR; (2) the water-leaving reflectance will be magnitude affected by the total scattered radiance which directly related to the type of the suspended sediments; (3) the difference between Spot 6 imagery-derived R_{rs} and the field spectral measurement (Figure 7-6) caused by the radiance correction (atmospheric correct)and time interval. The affected by the first two points is related to the specific inherent optical properties (IOPs) and environmental conditions of the water of the Kristalbad, therefore, need to be scrutinized and reinitialized. For the influence by the third point, due to the field measurement was taken during the Spot 6 overpass time, the affected by the time interval is negligible. Therefore the deviation between the Spot 6 imagery-derived R_{rs} and the field spectral measurement is mainly caused by the radiance correction, in this research mainly is the atmospheric correction. In the Figure 7-6, the difference in the blue band and the green band is larger than in the red band and NIR band and this will lead to the low accurate of the inversion. Because the empirical algorithm we adopted in this research is the blue-red-NIR three-band model, the reflectance in the blue band plays an important role in the C_{chla} inversion. Hence, the efficiency of the inversion could be improved when a better atmospheric correction could be developed and other uncertain factors (specific IOPs and environmental conditions) could be investigated well.

Table 7-3 The estimation error between the laboratory-measured and Spot 6 derived Chl-a conc.

Sample code	Laboratory-measured Chl-a (mg m^{-3})	Imagery-derived Chl-a (mg m-3)	Δ(difference)	RMSE	RPD
SK1	147.97	140.67	-7.30	31.3	4.39
SK2	187.94	173.89	-14.05	-	-
SK3	257.03	281.47	24.43		
SK4	143.84	101.38	-42.46		
SK5	114.17	119.19	5.02		
SK6	120.51	152.26	31.76		
SK7	502.54	446.06	-56.48		

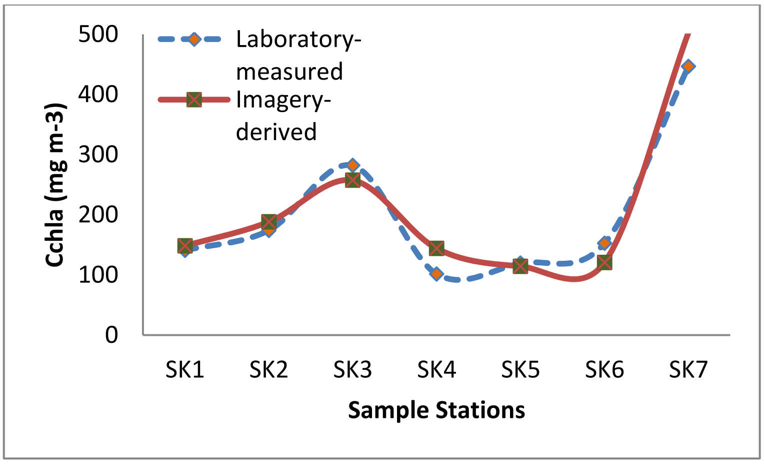

Figure 7-4 Comparison between laboratory-measured and Imagery-derived data

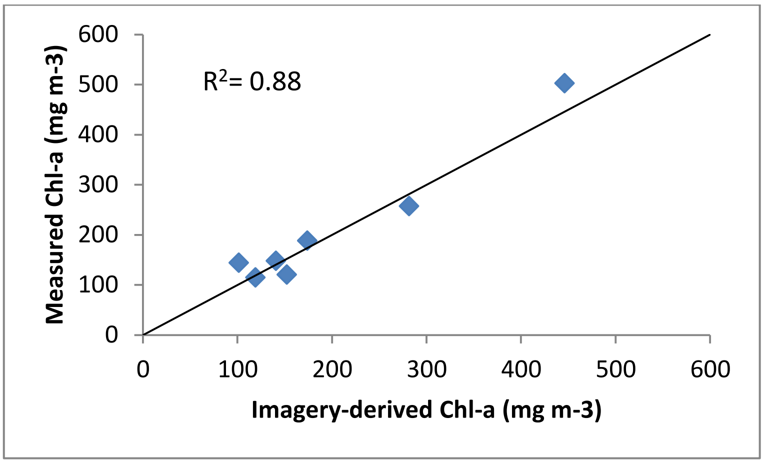

Figure 7-5 Comparison between laboratory-measured and Imagery-derived data

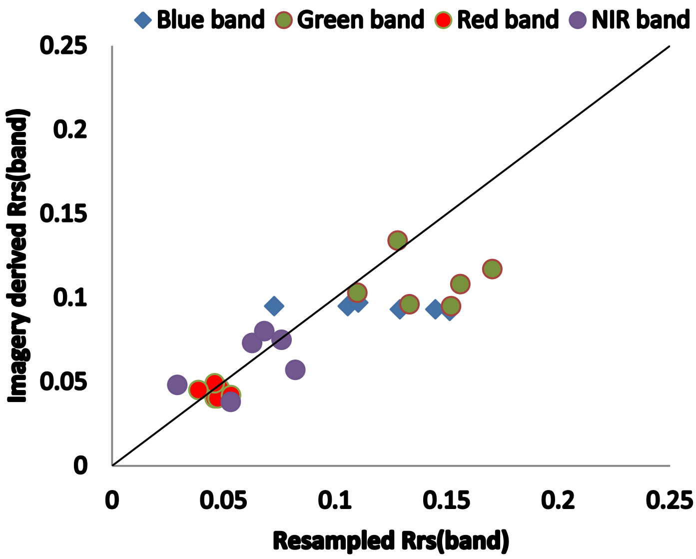

Figure 7-6 Comparison between the measured R_{rs} (i) and the Spot 6 derived R_{rs} (i) on 1st October 2015

7.4. Chl-a concentration modelling integrated with remote sensing

The Chl-*a* concentrations of the Kristalbad, from the inlet injected with the Elsbeek stream to three wetland ponds then gather in the outlet, were simulated by a one-dimensional water quality model, DUFLOW. Remote sensing was applied to the calibration process of chlorophyll-a modelling in the form of the estimated chl-a data. Calibrated data were performed by 9 estimated datasets (4 for pond 1, 3 for pond 2, and 2 for pond 3) from the image. The model results for chlorophyll-a for each pond give the similar trend of the concentration values which were derived from the Spot 6 image (an example for pond 1 was shown in Figure 7-7). For each pond (here is the pond 1) has three sections and in each section has different behavior for chlorophyll-a. from the first section to the section (50 m to 250 m), the chlorophyll-a concentration increases from 100 to 150 mg $^{-3}$, and keeps an steady state in about 150 mg $^{-3}$, in from section 2 to section 3 (250 m to 400 m), then in the last section (from 400 m to 800 m) the value drastic increases from 150 to 250 mg $^{-3}$.

After calibration, the simulated Chl-a spatial distribution in the steady state in three ponds of the Kristalbad on the 1st October 2015 could be seen in Figure 7-8. The level of the simulated chl-a concentrations is range from 100 to 250 mg m^{-3} and gently increased from the inlet to the outlet in each pond. From the graph, the curve for each pond has the downward trend in some positions which are the location of the weirs. Due to the weir could change the water level and discharge to reduce the nutrients load, therefore, the concentration of the Chl-a concentrations were affected by these structures.

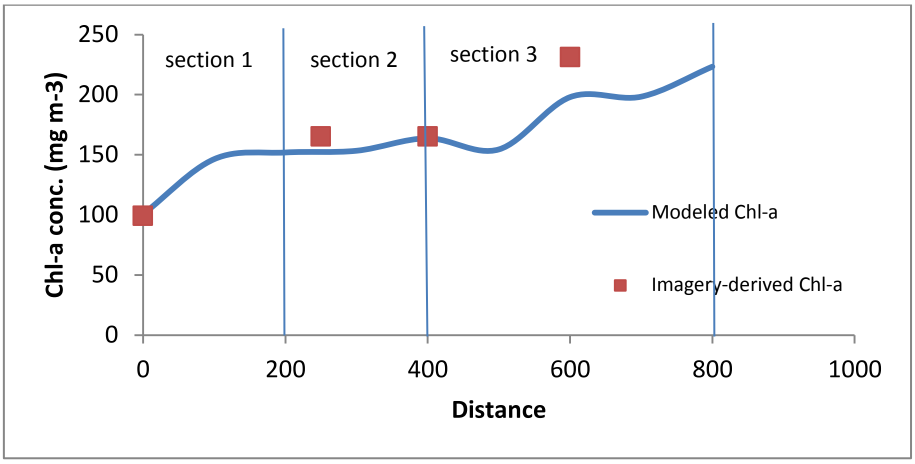

Figure 7-7 Comparison between modeled Chl-a with the imagery-derived Chl-a for Pond 1.

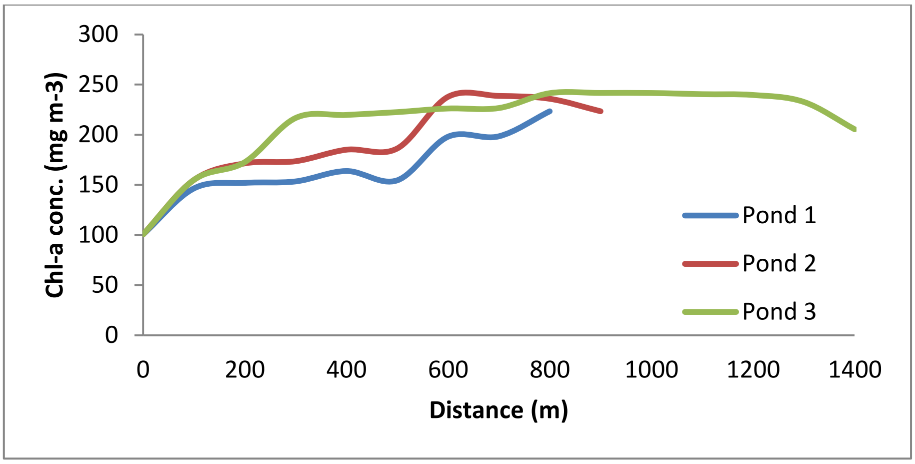

Figure 7-8 DUFLOW modelled Chl-a concentration in each pond of Kristalbad

7.5. Chl-a concentration prediction

The one month predictions for the Chl-a concentration dynamics in three ponds of Kristalbad from 1st October to 1St November are worked out in Figure 7-9. Overall, level of Chl-a concentration is range from 60 to 400 mg m^{-3} in Kristalbad but the level of concentration in pond 3 is higher than it in other two ponds. Figure 7-9 shows the trends of C_{cha} dynamic change for each pond are quite similar, (1) from 1st to 8th October 2015 it could be seen a positive trend; (2) at 15th, the concentration of chlorophyll-a reached peak (above 320 mg m^{-3}); (3) from 16th to the end, showed an obviously decrease trend.

Due to the phytoplankton activities are significant influenced by the intensity of photosynthesis which is sensitive to the weather conditions. Therefore, these dynamic changes could be attributed to the influence by the light energy and the temperature conditions. Figure 7-10 and 7-11 show the relationship between predicted Chl-a concentrations with light energy and temperature from 1st October to 1st November 2015, respectively. During the prediction period, the light energy ranges from 0 to 650 W.m^{-2}, and the temperature is between 1 **°C** and 18 **°C**. It could be seen that, light energy and the water temperature could directly affect the concentration of chlorophyll-a, but at around 14th October 2015, temperature has an opposite effect on C_{cha}. This phenomenon illustrated that the light energy is a major factor on phytoplankton growth for Kristalbad.

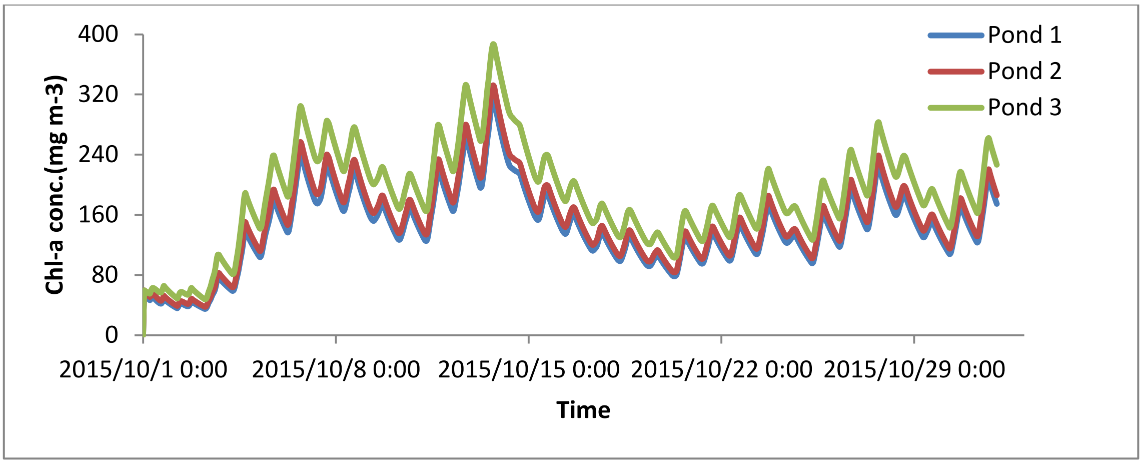

Figure 7-9 DUFLOW modeled Chl-a conc. in Kristalbad from 1st October to 1St November 2015.

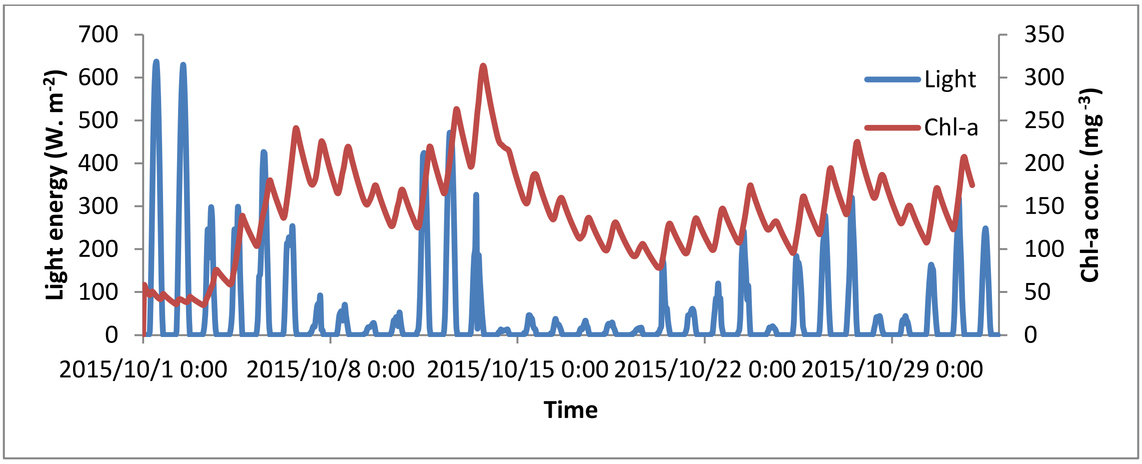

Figure 7-10 Relationship between DUFLOW modelled Chl-a conc. with light energy, an example in pond 1.

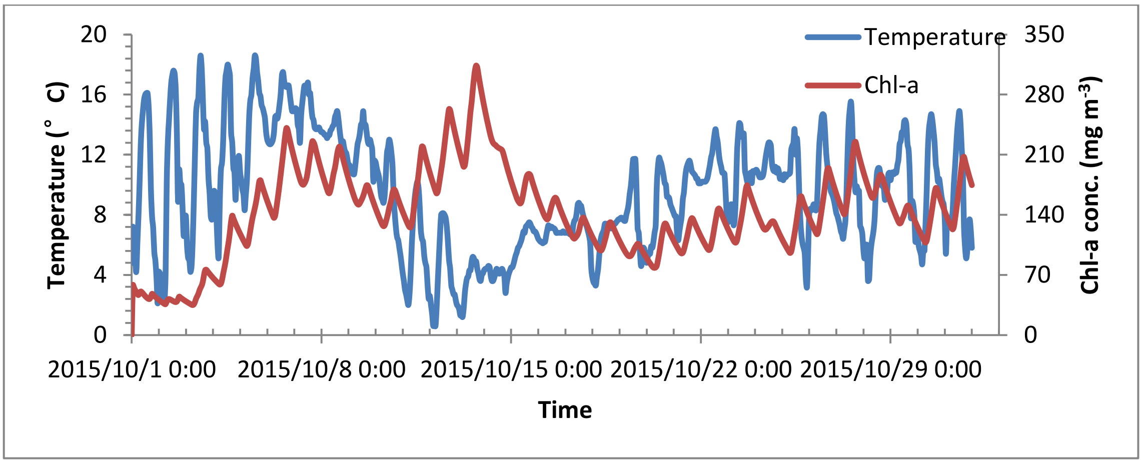

Figure 7-11 Relationship between DUFLOW modelled Chl-a conc. with water temperature, an example in pond 1.

8. CONCLUSIONS AND RECOMMENDATIONS

8.1. Overall conclusion

In order to know about the behaviour of the phytoplankton in Kristalbad, a water quality mapping and modelling approach integrating a SPOT 6 high spatial resolution image, field measurements of the surface reflectance, laboratory measurement of Chl-a concentrations, and DUFLOW water quality model was adopted in this research. For retrieval of the Chl-a in Kristalbad wetland, an empirical algorithm based on three-wide bands of SPOT6 and collected field data was developed. In general, in productive and optical shallow inland water, we considered the two band ratio model based on the red and NIR band which are located in 670 nm and 710 nm, respectively. Due that these two bands are primary sensitive to the chlorophyll pigments. In this research, such small, shallow, and productive inland water, only the high-spatial resolution image (± 5 m) was appropriate for the Kristalbad. Therefore the SPOT 6 satellite data with only four bands adopted to map the spatial distribution of the Chl-a concentration. Meanwhile, a recent proposed three- band model adopting blue-red-NIR spectral channels used for Landsat ETM+ was applied for deriving the Chl-a. This best-fitted three-band model was applied to SPOT 6 image of Kristalbad taken on 1st October 2015 to generate distribution map of Chl-a. Although using remote sensing images with high spatial resolution has the feasibility of rapid retrieving and monitoring Chl-a distribution in the certain area, it is difficult to use in modelling and predicting the environmental changes. But remote sensing application, such as forecasting, could be expanded through integration with the traditional modelling and GIS techniques to enhance the simulation performance of water qualities. Therefore, the imagery-derived Chl-a data with the hydraulic data were applied in the DUFLOW water quality modelling. Due to limited number of the measured Chl-a data, the imagery-derived C_{cha} were flexible used to calibrate the simulation results and this performed well in this research. With the help of the DUFLOW water quality model, the spatial distribution of C_{cha} in each pond in Kristalbad could be simulated. When the time series data of the environmental conditions have been set in the DUFLOW model, a prediction of Chl-a concentrations dynamics for each pond in Kristalbad from 1st October to 1st November 2015 could has been modelled. The principal conclusions for this research are as follows:

(1) In the study area, a wide range of $\mathrm{C_{cha}}$ were observed, with the ranges from 114.17 to 502.54 mg m-3, which were used to develop the regression model.
(2) Results from the regression modelling that the three -band model adopting blue-red-NIR spectral channels is the best-fitted model for $\mathrm{C_{cha}}$ retrieval. The regression model gives good retrievals for Chl-a, with RMSE of 23.4 mg m-3.
(3) After applying the best-fitted regression model on the Spot 6 image, the Chl-a concentrations can be derived from the image with RMSE of 31.3. The estimation accuracy could be enhanced by improving the accuracy of the atmospheric correction and surface reflectance data in the future.
(4) When matching the location information between the Chl-a distribution map and measured data at each sampling site, the map showed a similar level with the measured data. Near the bank of the ponds, the level of $\mathrm{C_{cha}}$ is higher than in the centre area this was caused by the adjacency effect.
(5) The imagery-derived Chl-a data with the hydraulic data were expansively applied to the DUFLOW water quality modelling (EUTROF 1). The imagery-derived $\mathrm{C_{cha}}$ were flexible used to calibrate the simulation results and could perform as well.
(6) The modelled $\mathrm{C_{cha}}$ for each pond in Kristalbad showed a similar range with the SPOT 6 derived Chl-a data from 100 to 250 mg m-3 and gently increased from the inlet to the outlet in each pond.
(7) A prediction of Chl-a concentrations dynamics for each pond in Kristalbad from 1st October to 1st November 2015 also has been modelled, and the $\mathrm{C_{cha}}$ showed a range from 80 to 400 mg m-3.

(8) By comparing the impact of light energy and water temperature on the C_{cha}, respectively, it can be concluded that light energy variation are the major factor on phytoplankton growth for Kristalbad.
(9) Combination with Image derived results and prediction model results could be used as a guiding analytical tool to provide information covering the entire study area and help to make policies, even a lower accuracy than the measured data.

8.2. Recommendations

The following recommendations can be made both on the basis of the experimental design and specific future research.

1. Overall, C_{cha} estimation integrating the remote sensing images of high spatial resolution and the water surface reflectance are feasible for rapid monitoring and modelling of the C_{cha}, but we still need to improve the estimation accuracy. The impact of SPM, CDOM, or nutrients in wetland waters for C_{cha} estimation should be further quantified.
2. The performance of the best-fitted algorithmic model could be improved adopting advanced four-band model and variation three-band model with the feasibility of the multispectral sensors, such as HYPERION(Chen, Zhang, & Quan, 2013).
3. A simple eutrophication model approach was used to simulated Chl-a and algae concentration. A more complex ecological water quality model would be used to present the real wetland eutrophication conditions.
4. The Duflow water quality modelling accuracy could be improved by considering more environmental changes, such as the water discharges, precipitation, and water storage.
5. It should be noted that in the future research, the monitoring and modelling was only validated in Kristalbad for one season (autumn). In order to optimize the uncertainty of the research, it is imperative to consider different environmental regimes and seasons.

9. REFERENCES

Abbott, M. B. (1979). *Computational Hydraulics: Elements of the Theory of Free Surface Flows*. Retrieved from https://books.google.nl/books/about/Computational_Hydraulics.html?id=v2YYAQAAIAAJ&pgis=1

Anderson, D. M., Glibert, P. M., & Burkholder, J. M. (2002a). Harmful algal blooms and eutrophication: Nutrient sources, composition, and consequences. *Estuaries*, *25*(4), 704–726. http://doi.org/10.1007/BF02804901

Anderson, D. M., Glibert, P. M., & Burkholder, J. M. (2002b). Harmful algal blooms and eutrophication: Nutrient sources, composition, and consequences. *Estuaries*, *25*(4), 704–726. http://doi.org/10.1007/BF02804901

Arar, E. (1997). Method 446.0: In vitro determination of chlorophylls a, b, c1+ c2 and pheopigments in marine and freshwater algae by visible spectrophotometry. Retrieved from https://scholar.google.com/scholar?q=+Method+446.0%3A+In+vitro+determination+of+chlorophylls+a%2C+b%2C+c1%2B+c2+and+pheopigments+in+marine+and+freshwater+algae+by+visible+spectrophotometry&btnG=&hl=zh-CN&as_sdt=0%2C5#0

ARMSTRONG, W. (1964). Oxygen Diffusion from the Roots of Some British Bog Plants. *Nature*, *204*(4960), 801–802. http://doi.org/10.1038/204801b0

Bissonnette, G., & Skousen, J. (2001). Treatment of domestic wastewater by three plant species in constructed wetlands. *Water, Air, and Soil Pollution*, *128*, 283–295.

Borg, R. (n.d.). Evaluatie van de nazuiverende functie van het Kristalbad: een onderzoek naar de werking en mogelijkheden voor optimalisatie van het vloeiveld in het Kristalbad.

Bosc, E. (2004). Seasonal and interannual variability in algal biomass and primary production in the Mediterranean Sea, as derived from 4 years of SeaWiFS observations. *Global Biogeochemical Cycles*, *18*, 1–17. http://doi.org/10.1029/2003GB002034

Campbell, J. (2002). Introduction to remote sensing. Retrieved from https://scholar.google.com/scholar?q=introduction+to+remote+sensing&btnG=&hl=zh-CN&as_sdt=0%2C5#0

Chang, C.-H., Liu, C.-C., Wen, C.-G., Cheng, I.-F., Tam, C.-K., & Huang, C.-S. (2009). Monitoring reservoir water quality with Formosat-2 high spatiotemporal imagery. *Journal of Environmental Monitoring : JEM*, *11*(11), 1982–1992. http://doi.org/10.1039/b912897b

Chen, J., Zhang, X., & Quan, W. (2013). Retrieval chlorophyll-a concentration from coastal waters: three-band semi-analytical algorithms comparison and development. *Optics Express*. Retrieved from https://www.osapublishing.org/abstract.cfm?uri=oe-21-7-9024

Choe, E., Lee, J., & Cheon, S. (2015). Monitoring and modelling of chlorophyll-a concentrations in rivers using a high-resolution satellite image : a case study in the Nakdong river , Korea, *1161*(November). http://doi.org/10.1080/01431161.2014.995270

Courault, D., Bsaibes, A., Kpemlie, E., Hadria, R., Hagolle, O., Marloie, O., … Desfonds, V. (2008). Assessing the potentialities of FORMOSAT-2 data for water and crop monitoring at small regional scale in South-Eastern France. *Sensors*, *8*(5), 3460–3481. http://doi.org/10.3390/s8053460

Dekker, A. G., Hoogenboom, H. J., Goddijn, L. M., & Malthus, T. J. M. (1997). Relation between inherent optical properties and reflectance spectra in turbid inland waters. *Remote Sensing Reviews*, *15*(January), 59–74. http://doi.org/10.1080/02757259709532331

Emy Chan, Taras A. Bursztynsky, Norman Hantzsche, A. Y. J. L. (1982). The use of wetlands for water pollution control. Mnicipal Environmental research Laboratory. Retrieved from EPA-600/S2-82-086

Falkowski, P. G. (1994). The role of phytoplankton photosynthesis in global biogeochemical cycles. *Photosynthesis Research*, *39*(3), 235–58. http://doi.org/10.1007/BF00014586

Fisher, J., & Acreman, M. (2004). Wetland nutrient removal: a review of the evidence. *Hydrology and Earth System …*. Retrieved from https://hal.archives-ouvertes.fr/hal-00304953/

Gersberg, R. M., Elkins, B. V., Lyon, S. R., & Goldman, C. R. (1986). Role of aquatic plants in wastewater treatment by artificial wetlands. *Water Research*, *20*(3), 363–368. http://doi.org/10.1016/0043-1354(86)90085-0

Gitelson, A. a., Dall'Olmo, G., Moses, W., Rundquist, D. C., Barrow, T., Fisher, T. R., … Holz, J. (2008). A simple semi-analytical model for remote estimation of chlorophyll-a in turbid waters: Validation. *Remote Sensing of Environment*, *112*(9), 3582–3593. http://doi.org/10.1016/j.rse.2008.04.015

Hamilton, D. P., & Schladow, S. G. (1997). Prediction of water quality in lakes and reservoirs. Part I — Model description. *Ecological Modelling*, *96*(1-3), 91–110. http://doi.org/10.1016/S0304-3800(96)00062-2

Hole, W., & Brook, S. (1982). Seasonal Variations in the Utilization of Ammonium and Nitrate by Phytoplankton in Vineyard Sound, Massachusetts, USA*, *249*, 237–249.

Iamchaturapatr, J., Yi, S. W., & Rhee, J. S. (2007). Nutrient removals by 21 aquatic plants for vertical free surface-flow (VFS) constructed wetland. *Ecological Engineering*, *29*(3), 287–293. http://doi.org/10.1016/j.ecoleng.2006.09.010

ICIM, D. (1992). A Micro-Computer Package for the Simulation of Unsteady Flow and Water Quality Processes in One-Dimensional Channel Systems. *Bureau ICIM, Rijswijk*. Retrieved from https://scholar.google.com/scholar?cluster=15268884261566436081&hl=zh-CN&as_sdt=2005&sciodt=0,5#0

Jong, J. de. (1976). purification of wastewater with the aid of rush or reed ponds. *Biological Control of Water Pollution. J. Tourbier & R.w. Pierson, Jr., Eds*. Retrieved from http://agris.fao.org/agris-search/search.do?recordID=US201303054240

Kahru, M., & Mitchell, B. G. (1999). Empirical chlorophyll algorithm and preliminary SeaWiFS validation for the California Current. *International Journal of Remote Sensing*, *20*(17), 3423–3429. http://doi.org/10.1080/014311699211453

Kottek, M., Grieser, J., Beck, C., Rudolf, B., & Rubel, F. (2006). World map of the Köppen-Geiger climate classification updated. *Meteorologische Zeitschrift*, *15*(3), 259–263. http://doi.org/10.1127/0941-2948/2006/0130

Lee, Z. P., Carder, K. L., Steward, R. G., Peacock, T. G., Davis, C. O., & Patch, J. S. (1998). An empirical algorithm for light absorption by ocean water total absorption coefficients ranging and modeled number of samples absorption the chlorophyll a concentrations to the spectral ratios and obtained results indicate that it is more accurate to est. *Journal of Geophysical Research*, *103*(98), 27967–27978.

Lim, J., & Choi, M. (2015). Assessment of water quality based on Landsat 8 operational land imager associated with human activities in Korea. *Environmental Monitoring and Assessment*, *187*, 1–17. http://doi.org/10.1007/s10661-015-4616-1

Liu, L., & Cheng, Z. (2010). Detection of vegetation light-use efficiency baseed on solar-induced chlorophyll fluorescence separarted from canopy radiance spectrum. *IEEE Journal of Selected Topics in Applied Earth Observations and Remote Sensing*, *3*(3), 306–312. http://doi.org/10.1109/JSTARS.2010.2048200

Luoheng, H., & Rundquist, D. C. (1997). Comparison of NIR/RED ratio and first derivative of reflectance in estimating algal-chlorophyll concentration: A case study in a turbid reservoir. *Remote Sensing of Environment*, *62*(3), 253–261. http://doi.org/10.1016/S0034-4257(97)00106-5

Ma, R., & Dai, J. (2005). Investigation of chlorophyll-a and total suspended matter concentrations using Landsat ETM and field spectral measurement in Taihu Lake, China. *International Journal of Remote Sensing*, *26*(13), 2779–2795. http://doi.org/10.1080/01431160512331326648

Mobley, C. D. (1999). Estimation of the remote-sensing reflectance from above-surface measurements. *Applied Optics*, *38*(36), 7442–7455. http://doi.org/10.1364/AO.38.007442

Moses, W. J., Gitelson, a a, Berdnikov, S., & Povazhnyy, V. (2009). concentration in case II waters using MODIS and MERIS data—successes and challenges. *Environmental Research Letters*, *4*(4), 045005. http://doi.org/10.1088/1748-9326/4/4/045005

Nichols, D. S. (1983). Capacity of Natural Wetlands to Remove Nutrients from Wastewater. *Journal - Water Pollution Control Federation*, *55*(5), 495–505. http://doi.org/10.2307/25041910

O'Reilly, J. E., Maritorena, S., Mitchell, B. G., Siegel, D. A., Carder, K. L., Garver, S. A., … McClain, C. (1998). Ocean color chlorophyll algorithms for SeaWiFS. *Journal of Geophysical Research*, *103*(C11), 24937. http://doi.org/10.1029/98JC02160

O'Reilly, J., & Maritorena, S. (2000). Ocean color chlorophyll a algorithms for SeaWiFS, OC2, and OC4: Version 4. *SeaWiFS Postlaunch …*, 8–22. Retrieved from http://www.spg.ucsd.edu/People/Mati/2000_OReilly_et_al_OC4v4_11-Chapt2.pdf

Odermatt, D., Gitelson, A., Brando, V. E., & Schaepman, M. (2012). Review of constituent retrieval in optically deep and complex waters from satellite imagery. *Remote Sensing of Environment*, *118*, 116–126. http://doi.org/10.1016/j.rse.2011.11.013

Res, W., Britain, G., Loma, A., Diego, S., Water, R., Agency, R., … July, R. (1983). Nitrogen removal in artificial wetlands, *17*(9), 14–19.

Schilling, K., & Zhang, Y.-K. (2004). Baseflow contribution to nitrate-nitrogen export from a large, agricultural watershed, USA. *Journal of Hydrology*, *295*(1-4), 305–316. http://doi.org/10.1016/j.jhydrol.2004.03.010

Singh, K., Ghosh, M., Sharma, S. R., & Kumar, P. (2014). Blue – Red – NIR Model for Chlorophyll- a Retrieval in Hypersaline – Alkaline Water Using Landsat ETM + Sensor, *7*(8), 3553–3559.

Subramaniam, A., Brown, C. W., Hood, R. R., Carpenter, E. J., & Capone, D. G. (2001). Detecting Trichodesmium blooms in SeaWiFS imagery. *Deep Sea Research Part II: Topical Studies in Oceanography*, *49*(1-3), 107–121. http://doi.org/10.1016/S0967-0645(01)00096-0

Tóth, L. (1972). Reeds control eutrophication of balaton lake. *Water Research*, *6*(12), 1533–1539. http://doi.org/10.1016/0043-1354(72)90076-0

Tyler, A. N., Svab, E., Preston, T., Présing, M., & Kovács, W. A. (2006). Remote sensing of the water quality of shallow lakes: A mixture modelling approach to quantifying phytoplankton in water characterized by high-suspended sediment. *International Journal of Remote Sensing*, *27*(8), 1521–1537. http://doi.org/10.1080/01431160500419311

van den Boomen, R., & Kampf, R. (2013). Waterharmonica's in Nederland (1996-2012), *2013*(07), 102.

Vieira, J. (1998). Eutrophication vulnerability analysis: a case study. *Water Science and Technology*, *37*(3), 121–128. http://doi.org/10.1016/S0273-1223(98)00063-8

Vymazal, J. (2007). Removal of nutrients in various types of constructed wetlands. *Science of the Total Environment*, *380*(1-3), 48–65. http://doi.org/10.1016/j.scitotenv.2006.09.014

Yang, M. D., Sykes, R. M., & Merry, C. J. (2000). Estimation of algal biological parameters using water quality modelling and SPOT satellite data, *125*, 1–13.

10. APPENDIX

Appendix 1 Map of the WWTP Enschede West

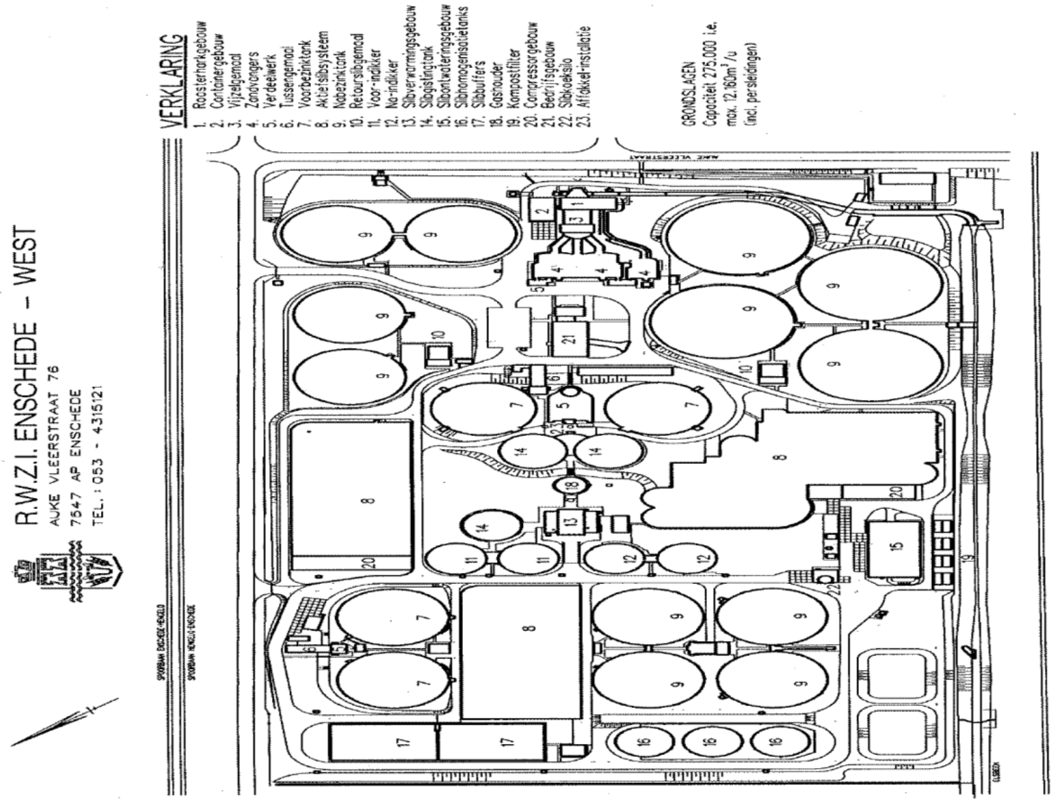

Appendix 2 Map of the cross sections of Kristalbad

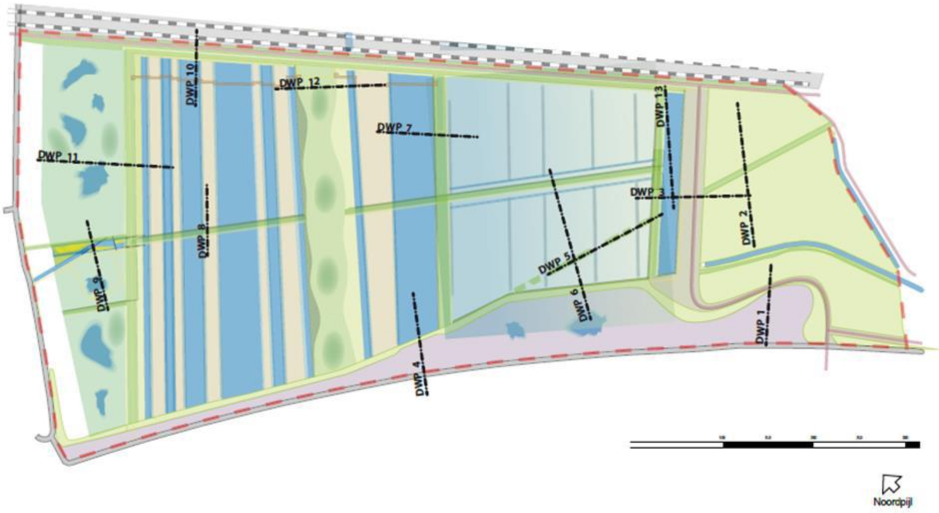

Appendix 3 the parameters of EUTRO 1 water quality model

Parameters	**Default**	**Dimension**	**Description**
k_p	[0.005]	mg-P/l	Monod constant Phosphorus
k_n	[0.010]	mg-N/l	Monod constant Nitrogen
e_{alg}	[0.016]	ug-Chl/l,m	Specific extinction chlorophyll
e_0	[1.000]	1/m	Background extinction
a_{chlc}	[30.000]	ug-Chl/mg-C	Chlorophyll to Carbon ratio
I_s	[40.000]	W/m^2	Optimal Light Intensity
u_{max}	[4.000]	1/day	Unlimited algal growth rate
t_{ga}	[1.047]	-	Temperature coefficient algal growth
t_{ra}	[1.047]	-	Temperature coefficient algal respiration
k_{res}	[0.100]	1/day	Respiration rate constant
k_{die}	[0.200]	1/day	Die rate constant
f_{porg}	[1.000]	-	Fraction PORG released by respiration
a_{pc}	[0.025]	mg-P/mg-C	Phosphorus to Carbon ratio
a_{nc}	[0.250]	mg-N/mg-C	Nitrogen to Carbon ratio
k_{min}	[0.100]	1/day	Rate constant mineralization
t_{min}	[1.047]	-	Temperature coefficient mineralization
v_{so}	[0.100]	m/day	Nett settling rate organic matter
f_{dporg}	[0.000]	-	Fraction dissolved organic Phosphorus
f_{dnorg}	[0.000]	-	Fraction dissolved organic Nitrogen
k_{pip}	[0.010]	l/mg-SS	Phosphorus Partition coefficient
f_{norg}	[1.000]	-	Fraction NORG released by respiration
k_{mn}	[0.025]	mg-N/l	Ammonia preference factor
t_{nit}	[1.080]	-	Temperature coefficient nitrification
k_{nit}	[0.100]	1/day	Nitrification rate constant
k_{no}	[2.000]	mg-O^2/l	Monod constant nitrification
k_{den}	[0.100]	1/day	Denitrification rate constant
t_{den}	[1.045]	-	Temperature coefficient denitrification
k_{dno}	[0.500]	mg-O^2/l	Monod constant denitrification
k_{bod}	[0.100]	1/day	Oxidation rate constant BOD
t_{bod}	[1.047]	-	Temperature coefficient oxidation BOD
k_{bodo}	[2.000]	mg-O^2/l	Monod constant oxidation BOD
f_{dbod}	[1.000]	-	Fraction dissolved BOD
a_{oc}	[2.670]	mg-O^2/mg-C	Oxygen to Carbon ratio
θ_{rea}	[1.024]	-	Temperature coefficient reaeration
k_{rmin}	[0.100]	m/day	Minimum oxygen mass transfer constant
v_{ss}	[0.100]	m/day	Sedimentation rate Suspended Solids

Appendix 4 Hourly light energy and water temperature data from 1st October to 1st November 2015

Date	Time	light energy ($w.m^{-2}$)	Temperature (°C)
20151001	0:00:00	0	7.1
	0:01:00	0	7.2
	0:02:00	0	4.8
	0:03:00	0	5.1
	0:04:00	0	4.2
	0:05:00	0	6.1
	0:06:00	9.4	8
	0:07:00	119.8	10.2
	0:08:00	282.9	12.7
	0:09:00	448.9	14.1
	0:10:00	562.6	15
	0:11:00	625.6	15.7
	0:12:00	636.6	16
	0:13:00	591.4	16.1
	0:14:00	496.2	16.1
	0:15:00	361.1	15.2
	0:16:00	205.7	13.1
	0:17:00	60.4	9.7
	0:18:00	0	7.9
	0:19:00	0	7.1
	0:20:00	0	5.5
	0:21:00	0	4.9
	0:22:00	0	3.7
	0:23:00	0	2.1
20151002	0:00:00	0	4.2
	0:01:00	0	4.1
	0:02:00	0	2.9
	0:03:00	0	2.5
	0:04:00	0	2.8
	0:05:00	0	2.2
	0:06:00	9.5	4.1
	0:07:00	124.1	10.2
	0:08:00	274.7	12.9
	0:09:00	404.7	14.3
	0:10:00	525.8	15.7
	0:11:00	599.7	16.8
	0:12:00	629.5	17.3
	0:13:00	584.9	17.6
	0:14:00	496.3	17.4
	0:15:00	369.3	16.3
	0:16:00	212.7	13.3
	0:17:00	62.0	8.9
	0:18:00	0	11

	0:19:00	0	10.1
	0:20:00	0	10
	0:21:00	0	8.5
	0:22:00	0	6.6
	0:23:00	0	7.5
20151003	0:00:00	0	7.9
	0:01:00	0	5.9
	0:02:00	0	5.1
	0:03:00	0	5
	0:04:00	0	4.2
	0:05:00	0	4.6
	0:06:00	5.3	6.3
	0:07:00	23.2	8.9
	0:08:00	62.9	12
	0:09:00	173.7	14.8
	0:10:00	246.4	15.5
	0:11:00	180.3	15.8
	0:12:00	233.3	17.7
	0:13:00	297.7	18.6
	0:14:00	266.3	17.7
	0:15:00	143.9	15.7
	0:16:00	67.8	13.7
	0:17:00	14.9	14.2
	0:18:00	0	12.8
	0:19:00	0	12.4
	0:20:00	0	10.4
	0:21:00	0	9.4
	0:22:00	0	7.9
	0:23:00	0	7.7
20151004	0:00:00	0	9.5
	0:01:00	0	9.6
	0:02:00	0	9.4
	0:03:00	0	7.9
	0:04:00	0	6
	0:05:00	0	5.2
	0:06:00	5.3	8.9
	0:07:00	23.2	11
	0:08:00	62.9	11.5
	0:09:00	173.7	13
	0:10:00	246.4	15.5
	0:11:00	180.3	17.1
	0:12:00	193.3	17.6
	0:13:00	297.7	18
	0:14:00	266.3	17.7
	0:15:00	143.9	17.2

	0:16:00	67.8	13.5
	0:17:00	0	12.8
	0:18:00	0	11.1
	0:19:00	0	10.8
	0:20:00	0	9
	0:21:00	0	11.7
	0:22:00	0	11.7
	0:23:00	0	11.9
20151005	0:00:00	0	10.8
	0:01:00	0	10.3
	0:02:00	0	9.7
	0:03:00	0	9.3
	0:04:00	0	8.3
	0:05:00	0	9.3
	0:06:00	8.4	10.3
	0:07:00	44.3	12.3
	0:08:00	135.6	14.5
	0:09:00	140.9	15.6
	0:10:00	208.7	16
	0:11:00	367.8	17.1
	0:12:00	426.1	17.7
	0:13:00	422.6	18.6
	0:14:00	346.9	18.4
	0:15:00	234.8	17.5
	0:16:00	135.6	16.9
	0:17:00	28.7	16.1
	0:18:00	0	15.9
	0:19:00	0	15.3
	0:20:00	0	15.1
	0:21:00	0	14.8
	0:22:00	0	14.4
	0:23:00	0	13.5
20151006	0:00:00	0	13
	0:01:00	0	12.8
	0:02:00	0	12.7
	0:03:00	0	12.7
	0:04:00	0	12.8
	0:05:00	0	13
	0:06:00	5.9	13.5
	0:07:00	55.1	14.5
	0:08:00	141.5	14.6
	0:09:00	213.2	14.4
	0:10:00	215.1	14.8
	0:11:00	227.9	15.4
	0:12:00	210.0	16.1

	0:13:00	209.6	17.3
	0:14:00	253.7	17.5
	0:15:00	182.0	16.9
	0:16:00	80.9	16.6
	0:17:00	16.5	16.5
	0:18:00	0	16.6
	0:19:00	0	16.6
	0:20:00	0	16
	0:21:00	0	15.4
	0:22:00	0	14.9
	0:23:00	0	14.9
20151007	0:00:00	0	14.9
	0:01:00	0	15.1
	0:02:00	0	15
	0:03:00	0	14
	0:04:00	0	13.7
	0:05:00	0	12.8
	0:06:00	4.5	14.6
	0:07:00	7.0	15.4
	0:08:00	15.4	16.1
	0:09:00	21.0	16.6
	0:10:00	19.6	16.2
	0:11:00	40.6	16.4
	0:12:00	65.3	16.8
	0:13:00	72.8	16
	0:14:00	67.2	16.1
	0:15:00	91.0	15.2
	0:16:00	12.6	14.5
	0:17:00	11.2	14.3
	0:18:00	0	13.8
	0:19:00	0	13.7
	0:20:00	0	13.7
	0:21:00	0	13.8
	0:22:00	0	13.8
	0:23:00	0	13.6
20151008	0:00:00	0	13.5
	0:01:00	0	13.5
	0:02:00	0	13.4
	0:03:00	0	13.3
	0:04:00	0	13.3
	0:05:00	0	13.1
	0:06:00	3.0	13.3
	0:07:00	21.5	13.3
	0:08:00	44.8	13.6
	0:09:00	52.3	13.7

	0:10:00	55.1	13.9
	0:11:00	33.6	14
	0:12:00	50.2	14.5
	0:13:00	70.9	14.7
	0:14:00	46.7	14.9
	0:15:00	28.9	14.4
	0:16:00	11.2	13.7
	0:17:00	0	13.1
	0:18:00	0	12.6
	0:19:00	0	12.9
	0:20:00	0	12.5
	0:21:00	0	12.2
	0:22:00	0	12.1
	0:23:00	0	11.7
20151009	0:00:00	0	11.3
	0:01:00	0	11.3
	0:02:00	0	11
	0:03:00	0	10.9
	0:04:00	0	10.7
	0:05:00	0	10.7
	0:06:00	1.9	11.3
	0:07:00	3.6	12
	0:08:00	4.9	12.7
	0:09:00	13.4	13
	0:10:00	18.2	13.4
	0:11:00	17.6	14
	0:12:00	20.2	14.1
	0:13:00	22.5	14.9
	0:14:00	26.8	13.9
	0:15:00	28.0	14
	0:16:00	15.8	13.5
	0:17:00	3.0	12.9
	0:18:00	0	12.7
	0:19:00	0	13
	0:20:00	0	12.7
	0:21:00	0	12.3
	0:22:00	0	10.2
	0:23:00	0	11.6
20151010	0:00:00	0	11.5
	0:01:00	0	11.1
	0:02:00	0	10.8
	0:03:00	0	10.5
	0:04:00	0	9.8
	0:05:00	0	9.2
	0:06:00	2.3	9

	0:07:00	7.9	8.8
	0:08:00	20.9	9.3
	0:09:00	34.6	10.6
	0:10:00	26.7	12.1
	0:11:00	41.8	12.5
	0:12:00	33.9	13
	0:13:00	20.9	12.7
	0:14:00	52.6	12.1
	0:15:00	33.9	11.2
	0:16:00	15.9	9.1
	0:17:00	4.3	8
	0:18:00	0	7.1
	0:19:00	0	6.5
	0:20:00	0	6.3
	0:21:00	0	5.8
	0:22:00	0	5.3
	0:23:00	0	4.7
20151011	0:00:00	0	4.1
	0:01:00	0	3.6
	0:02:00	0	3
	0:03:00	0	2.7
	0:04:00	0	2.3
	0:05:00	0	2
	0:06:00	7.8	2.7
	0:07:00	14.6	4.1
	0:08:00	55.9	6
	0:09:00	145.9	7.4
	0:10:00	274.8	8.6
	0:11:00	415.9	9.4
	0:12:00	424.3	9.9
	0:13:00	403.7	10.2
	0:14:00	335.6	9.8
	0:15:00	235.9	8.6
	0:16:00	124.0	7
	0:17:00	21.9	6.4
	0:18:00	0	6.2
	0:19:00	0	5.3
	0:20:00	0	4.8
	0:21:00	0	4.5
	0:22:00	0	3.3
	0:23:00	0	2.4
20151012	0:00:00	0	2.6
	0:01:00	0	2
	0:02:00	0	1.4
	0:03:00	0	0.6

	0:04:00	0	0.9
	0:05:00	0	0.6
	0:06:00	8.4	1.8
	0:07:00	57.5	3.5
	0:08:00	185.7	5.1
	0:09:00	308.7	6.7
	0:10:00	413.3	8
	0:11:00	470.9	8.1
	0:12:00	470.9	8.1
	0:13:00	455.2	8
	0:14:00	379.3	7.8
	0:15:00	264.2	7.2
	0:16:00	130.8	6.2
	0:17:00	23.5	5
	0:18:00	0	4.4
	0:19:00	0	3.3
	0:20:00	0	3
	0:21:00	0	2.7
	0:22:00	0	2.7
	0:23:00	0	2.3
20151013	0:00:00	0	2
	0:01:00	0	1.9
	0:02:00	0	1.7
	0:03:00	0	1.3
	0:04:00	0	1.3
	0:05:00	0	1.2
	0:06:00	5.9	1.8
	0:07:00	44.5	2.8
	0:08:00	118.5	3.4
	0:09:00	181.5	3.8
	0:10:00	203.8	3.9
	0:11:00	322.3	4.3
	0:12:00	16.7	4.3
	0:13:00	181.5	4.9
	0:14:00	137.1	5.2
	0:15:00	94.5	5.1
	0:16:00	53.7	4.7
	0:17:00	24.1	4.9
	0:18:00	0	4.4
	0:19:00	0	4.1
	0:20:00	0	3.7
	0:21:00	0	3.6
	0:22:00	0	4
	0:23:00	0	4.1
20151014	0:00:00	0	4.3

	0:01:00	0	4.4
	0:02:00	0	4.4
	0:03:00	0	4.5
	0:04:00	0	4.6
	0:05:00	0	4.5
	0:06:00	1.3	3.9
	0:07:00	6.4	3.6
	0:08:00	7.2	3.6
	0:09:00	13.2	3.8
	0:10:00	8.8	4.1
	0:11:00	10.4	4.4
	0:12:00	10.4	4.3
	0:13:00	11.6	4.1
	0:14:00	11.2	4.1
	0:15:00	13.2	4.3
	0:16:00	6.0	4.4
	0:17:00	0.8	4.2
	0:18:00	0	3.9
	0:19:00	0	2.8
	0:20:00	0	3.4
	0:21:00	0	3.8
	0:22:00	0	4.1
	0:23:00	0	4.3
20151015	0:00:00	0	4.5
	0:01:00	0	4.5
	0:02:00	0	4.7
	0:03:00	0	5
	0:04:00	0	5.3
	0:05:00	0	5.5
	0:06:00	5.3	5.8
	0:07:00	3.3	5.9
	0:08:00	11.5	6.1
	0:09:00	26.2	6.3
	0:10:00	45.9	6.6
	0:11:00	45.9	6.9
	0:12:00	40.1	6.8
	0:13:00	37.7	7.2
	0:14:00	21.3	7.3
	0:15:00	14.8	7.4
	0:16:00	13.1	7.5
	0:17:00	1.6	7.4
	0:18:00	0	7.2
	0:19:00	0	7.1
	0:20:00	0	6.9
	0:21:00	0	6.9

	0:22:00	0	6.8
	0:23:00	0	6.6
20151016	0:00:00	0	6.4
	0:01:00	0	6.3
	0:02:00	0	6.2
	0:03:00	0	6.2
	0:04:00	0	6.1
	0:05:00	0	6.2
	0:06:00	4.5	6.2
	0:07:00	2.8	6.6
	0:08:00	12.6	7
	0:09:00	26.6	7.3
	0:10:00	37.8	7.1
	0:11:00	29.4	7.2
	0:12:00	25.8	7.2
	0:13:00	23.8	7.1
	0:14:00	18.2	7.1
	0:15:00	11.2	7
	0:16:00	2.8	6.8
	0:17:00	0.0	6.8
	0:18:00	0	6.8
	0:19:00	0	6.8
	0:20:00	0	6.8
	0:21:00	0	6.8
	0:22:00	0	6.9
	0:23:00	0	6.8
20151017	0:00:00	0	6.8
	0:01:00	0	6.8
	0:02:00	0	6.8
	0:03:00	0	6.9
	0:04:00	0	6.7
	0:05:00	0	6.7
	0:06:00	2.1	6.7
	0:07:00	2.0	7.3
	0:08:00	11.8	7.6
	0:09:00	15.8	7.7
	0:10:00	13.2	8.1
	0:11:00	20.4	8.7
	0:12:00	27.6	8.8
	0:13:00	33.6	8.6
	0:14:00	23.0	8.6
	0:15:00	17.8	8.2
	0:16:00	4.6	7.9
	0:17:00	0.7	7.6
	0:18:00	0	7.4

	0:19:00	0	7.2
	0:20:00	0	6.9
	0:21:00	0	6.6
	0:22:00	0	6.1
	0:23:00	0	4.4
20151018	0:00:00	0	3.8
	0:01:00	0	3.5
	0:02:00	0	3.4
	0:03:00	0	3.3
	0:04:00	0	3.9
	0:05:00	0	4.4
	0:06:00	4.2	5.3
	0:07:00	4.0	6.2
	0:08:00	14.6	6.6
	0:09:00	23.9	6.8
	0:10:00	26.5	7
	0:11:00	22.5	7.4
	0:12:00	26.2	7.4
	0:13:00	29.2	7.4
	0:14:00	18.6	7.4
	0:15:00	13.3	7.2
	0:16:00	5.3	7.1
	0:17:00	1.3	7.1
	0:18:00	0	7.2
	0:19:00	0	7.4
	0:20:00	0	7.4
	0:21:00	0	7.5
	0:22:00	0	7.6
	0:23:00	0	7.7
20151019	0:00:00	0	7.7
	0:01:00	0	7.8
	0:02:00	0	7.8
	0:03:00	0	7.7
	0:04:00	0	7.6
	0:05:00	0	7.6
	0:06:00	1.4	8
	0:07:00	1.3	8.3
	0:08:00	4.8	8.7
	0:09:00	5.7	9.4
	0:10:00	10.1	9.9
	0:11:00	13.5	10.8
	0:12:00	14.6	11.7
	0:13:00	16.2	11.4
	0:14:00	10.9	11.7
	0:15:00	17.5	9.8

	0:16:00	7.9	7.1
	0:17:00	0.9	6.8
	0:18:00	0	5.6
	0:19:00	0	4.6
	0:20:00	0	5
	0:21:00	0	5.8
	0:22:00	0	5.7
	0:23:00	0	5.2
20151020	0:00:00	0	4.8
	0:01:00	0	5.2
	0:02:00	0	5.5
	0:03:00	0	5.4
	0:04:00	0	5.9
	0:05:00	0	5.8
	0:06:00	5.2	6.2
	0:07:00	6.6	6.8
	0:08:00	14.8	7.3
	0:09:00	21.3	10
	0:10:00	175.5	11.2
	0:11:00	165.6	11.8
	0:12:00	98.8	11.6
	0:13:00	59.0	11.4
	0:14:00	62.3	11
	0:15:00	32.8	10.6
	0:16:00	14.8	10.1
	0:17:00	1.6	10
	0:18:00	0	9.2
	0:19:00	0	9.2
	0:20:00	0	9.1
	0:21:00	0	8.7
	0:22:00	0	8.5
	0:23:00	0	8.3
20151021	0:00:00	0	8.1
	0:01:00	0	7.9
	0:02:00	0	7.9
	0:03:00	0	6.7
	0:04:00	0	6.3
	0:05:00	0	6.9
	0:06:00	3.1	7.4
	0:07:00	7.8	7.9
	0:08:00	19.5	9
	0:09:00	45.7	9.5
	0:10:00	46.7	10.4
	0:11:00	49.6	11
	0:12:00	57.7	11.3

	0:13:00	61.3	11.5
	0:14:00	55.5	11.6
	0:15:00	36.0	11.3
	0:16:00	12.6	10.9
	0:17:00	1.0	10.8
	0:18:00	0	10.7
	0:19:00	0	10.6
	0:20:00	0	10.4
	0:21:00	0	10.4
	0:22:00	0	10.1
	0:23:00	0	10.1
20151022	0:00:00	0	10.1
	0:01:00	0	10.2
	0:02:00	0	10.2
	0:03:00	0	10.2
	0:04:00	0	10.2
	0:05:00	0	10.3
	0:06:00	3.1	10.5
	0:07:00	4.6	10.9
	0:08:00	32.4	11.3
	0:09:00	57.8	11.8
	0:10:00	85.6	12.1
	0:11:00	80.9	12.7
	0:12:00	120.3	13.3
	0:13:00	80.9	13.7
	0:14:00	85.6	13.2
	0:15:00	25.4	12.8
	0:16:00	9.2	12
	0:17:00	0	11.5
	0:18:00	0	11.2
	0:19:00	0	10.8
	0:20:00	0	10.8
	0:21:00	0	10.7
	0:22:00	0	9.3
	0:23:00	0	7.9
20151023	0:00:00	0	7.5
	0:01:00	0	7.6
	0:02:00	0	8.6
	0:03:00	0	8.7
	0:04:00	0	8.2
	0:05:00	0	7.3
	0:06:00	6.5	7.7
	0:07:00	12.1	9.4
	0:08:00	50.4	12.1
	0:09:00	171.4	13.3

	0:10:00	215.7	14.1
	0:11:00	241.9	14
	0:12:00	188.1	13.2
	0:13:00	145.2	13.2
	0:14:00	82.7	13.4
	0:15:00	114.9	11
	0:16:00	50.4	10.6
	0:17:00	2.0	10.2
	0:18:00	0	10.1
	0:19:00	0	10.3
	0:20:00	0	10.8
	0:21:00	0	10.1
	0:22:00	0	10.9
	0:23:00	0	10.8
20151024	0:00:00	0	10.9
	0:01:00	0	11
	0:02:00	0	10.9
	0:03:00	0	10.7
	0:04:00	0	10.5
	0:05:00	0	10.5
	0:06:00	0	10.5
	0:07:00	1.0	10.6
	0:08:00	5.0	11
	0:09:00	10.0	11.6
	0:10:00	17.5	12.1
	0:11:00	16.5	12.5
	0:12:00	18.8	12.8
	0:13:00	20.5	12.8
	0:14:00	17.0	12.6
	0:15:00	14.0	11.4
	0:16:00	8.5	11
	0:17:00	0.5	10.9
	0:18:00	0	11.2
	0:19:00	0	10.8
	0:20:00	0	11.1
	0:21:00	0	10.9
	0:22:00	0	10.4
	0:23:00	0	10.4
20151025	0:00:00	0	10.6
	0:01:00	0	10.3
	0:02:00	0	10.7
	0:03:00	0	10.5
	0:04:00	0	10.6
	0:05:00	0	10.7
	0:06:00	0	10.7

	0:07:00	4.7	10.8
	0:08:00	37.2	12.3
	0:09:00	125.6	12.6
	0:10:00	182.9	12.8
	0:11:00	167.4	13.7
	0:12:00	169.2	12
	0:13:00	156.6	13.1
	0:14:00	125.6	12.1
	0:15:00	83.7	9.7
	0:16:00	23.3	7.8
	0:17:00	10	6.7
	0:18:00	0	6.1
	0:19:00	0	5.8
	0:20:00	0	5.4
	0:21:00	0	3.7
	0:22:00	0	3.2
	0:23:00	0	5.5
20151026	0:00:00	0	8.2
	0:01:00	0	8.4
	0:02:00	0	8.3
	0:03:00	0	8.5
	0:04:00	0	8.7
	0:05:00	0	8.4
	0:06:00	0	8.3
	0:07:00	11.1	9
	0:08:00	66.6	11
	0:09:00	140.6	12.8
	0:10:00	207.2	13.6
	0:11:00	235.0	14.5
	0:12:00	278.5	14.7
	0:13:00	235.0	14.6
	0:14:00	175.8	13.5
	0:15:00	98.1	12.1
	0:16:00	37.0	11.3
	0:17:00	1.9	10.5
	0:18:00	0	10.1
	0:19:00	0	9.6
	0:20:00	0	9.4
	0:21:00	0	9.2
	0:22:00	0	8.9
	0:23:00	0	8.5
20151027	0:00:00	0	8.1
	0:01:00	0	7.9
	0:02:00	0	7.6
	0:03:00	0	7.3

	0:04:00	0	6.9
	0:05:00	0	6.7
	0:06:00	0	6.4
	0:07:00	8.1	7
	0:08:00	50.5	7.6
	0:09:00	101.0	9.5
	0:10:00	159.6	12.3
	0:11:00	280.8	14.2
	0:12:00	320.2	15.1
	0:13:00	260.6	15.5
	0:14:00	202.0	14.1
	0:15:00	123.2	11.6
	0:16:00	38.4	10.3
	0:17:00	0	9.5
	0:18:00	18	9.9
	0:19:00	18	9.6
	0:20:00	18	9.6
	0:21:00	13	7.3
	0:22:00	13	7.1
	0:23:00	12	6.7
20151028	0:00:00	0	5.6
	0:01:00	0	5.1
	0:02:00	0	6
	0:03:00	0	6
	0:04:00	0	3.6
	0:05:00	0	3.7
	0:06:00	0	5.2
	0:07:00	2.4	6
	0:08:00	15.2	6.5
	0:09:00	26.4	7
	0:10:00	41.6	7.9
	0:11:00	38.4	9.7
	0:12:00	41.8	10.8
	0:13:00	44.0	11.1
	0:14:00	32.0	11.1
	0:15:00	14.4	10.7
	0:16:00	5.6	10
	0:17:00	0	9.9
	0:18:00	18	9.8
	0:19:00	17	9
	0:20:00	17	9.3
	0:21:00	18	9.6
	0:22:00	20	10.7
	0:23:00	20	10.8
20151029	0:00:00	0	10.3

	0:01:00	0	10.8
	0:02:00	0	10.8
	0:03:00	0	10.7
	0:04:00	0	10.9
	0:05:00	0	10.8
	0:06:00	0	11.3
	0:07:00	1.1	11.7
	0:08:00	8.4	12.7
	0:09:00	30.2	12.9
	0:10:00	35.8	13.5
	0:11:00	26.9	13.4
	0:12:00	44.2	14.2
	0:13:00	35.8	14.3
	0:14:00	30.2	14
	0:15:00	18.5	12.7
	0:16:00	3.9	12.3
	0:17:00	0	10.7
	0:18:00	14	7.8
	0:19:00	16	8.9
	0:20:00	16	8.7
	0:21:00	15	8
	0:22:00	11	6.2
	0:23:00	11	6.2
20151030	0:00:00	0	6.6
	0:01:00	0	5.9
	0:02:00	0	5.6
	0:03:00	0	5.3
	0:04:00	0	4.7
	0:05:00	0	5.6
	0:06:00	0	5.6
	0:07:00	6.2	7.5
	0:08:00	55.4	9.6
	0:09:00	103.2	12.3
	0:10:00	138.6	13.7
	0:11:00	163.2	14.3
	0:12:00	157.4	14.7
	0:13:00	149.4	14.3
	0:14:00	92.4	13.6
	0:15:00	52.4	12.8
	0:16:00	18.5	11.4
	0:17:00	0	10.9
	0:18:00	19	10.2
	0:19:00	19	10.4
	0:20:00	18	9.9
	0:21:00	17	9.3

	0:22:00	16	8.9
	0:23:00	16	8.7
20151031	0:00:00	0	7.7
	0:01:00	0	5.4
	0:02:00	0	7.7
	0:03:00	0	7.7
	0:04:00	0	7.5
	0:05:00	0	7.7
	0:06:00	0	7.7
	0:07:00	7.8	8.3
	0:08:00	52.7	10
	0:09:00	140.4	11.1
	0:10:00	210.6	12.4
	0:11:00	257.4	13.6
	0:12:00	319.5	14.4
	0:13:00	234.0	14.9
	0:14:00	171.6	14
	0:15:00	83.9	12.4
	0:16:00	35.1	10.9
	0:17:00	0	7.2
	0:18:00	11	5.8
	0:19:00	9	5.1
	0:20:00	10	5.7
	0:21:00	13	7
	0:22:00	14	7.7
	0:23:00	13	7
20151101	0:00:00	0	5.8
	0:01:00	0	5
	0:02:00	0	5.6
	0:03:00	0	5.5
	0:04:00	0	5.2
	0:05:00	0	5.3
	0:06:00	0	6.3
	0:07:00	5.6	7.3
	0:08:00	53.7	9
	0:09:00	122.1	10.8
	0:10:00	183.2	12.4
	0:11:00	233.1	13.2
	0:12:00	238.5	14.2
	0:13:00	220.2	14.7
	0:14:00	161.0	14.7
	0:15:00	98.1	10.6
	0:16:00	25.9	7.6
	0:17:00	0	5.3
	0:18:00	0	4.1

	0:19:00	0	4.1
	0:20:00	0	2.8
	0:21:00	0	3
	0:22:00	0	3.2
	0:23:00	0	2.6